Nordic Seas Heat Loss, Atlantic Inflow, and Arctic Sea Ice cover over the last century

Lars H. Smedsrud [1]*, Ailin Brakstad [1]*, Erica Madonna [1]*, Morven Muilwijk [1]*, Siv K. Lauvset [2]*, Clemens Spensberger [1]*, Andreas Born [3]*, Tor Eldevik [1]*, Helge Drange [1]*, Emil Jeansson [2]*, Camille Li [1]*, Are Olsen [1]*, Øystein Skagseth [4]*, Donald A. Slater [5], Fiamma Straneo [6], Kjetil Våge [1] * and Marius Årthun [1]*.

[1] Geophysical Institute, University of Bergen, Norway.

[2] NORCE Norwegian Research Centre, Bergen Norway.

[3] Department for Earth Science, University of Bergen, Norway.

[4] Institute for Marine Research, Bergen, Norway.

[5] St. Andrews or University of Edinburg, Scotland, United Kingdom.

[6] Scripps Institution of Oceanography, UCSD, USA.

* Bjerknes Centre for Climate Research

Corresponding author: Lars H. Smedsrud (Lars.Smedsrud@uib.no)

Key Points:

- Nordic Seas heat loss dominates variability and mean Arctic Ocean heat loss
- Atlantic Water volume and heat transport has increased over the last century consistent with increased wind forcing and heat loss
- Ocean heat anomalies affect Greenland melting, Arctic sea ice, water transformations and Arctic CO_2 uptake.

Abstract

Poleward ocean heat transport is a key process in the earth system. We detail and review the northward Atlantic Water (AW) flow, Arctic Ocean heat transport and heat loss to the atmosphere since 1900, in relation to sea ice cover. Our synthesis is largely based on a sea ice-ocean model forced by a reanalysis atmosphere (1900-2018) corroborated by a comprehensive hydrographic database (1950-), AW inflow observations (1996-), and key long-term time series. The Arctic Seas, including the Nordic and Barents Seas, have warmed since the 1970s, especially on the shelves. This warming is congruent with increased ocean heat transport and sea ice loss, and has contributed to the retreat of marine terminating glaciers on Greenland. Heat loss to the atmosphere is largest in the Nordic Seas (60% of total): with large variability linked to the frequency of Cold Air Outbreaks and cyclones in the region, but the long-term positive trend is small. Heat loss from the Barents Sea (~30%) and Arctic Seas farther north (~10%) is overall smaller, but have large positive trends. The AW inflow, heat loss to the atmosphere, and dense outflow have thus all increased since 1900. These are consistently related through theoretical scaling, but the AW inflow increase is also wind-driven. The Nordic, Barents and other Arctic Seas CO_2 uptake constitutes ~8% of the global uptake and seems largely driven by heat loss. This uptake has increased by ~30% over the last century - consistent with Arctic sea ice loss allowing more regional air-sea interaction.

Plain Language Summary

The major flow to and from the Arctic Ocean occurs across the Greenland-Scotland Ridge. The inflow is mostly warm Atlantic Water (AW) flowing northwards and cooling gradually. This water eventually flows south as cold freshened Polar Water at the surface and cold dense Overflow Water at depth. We review and synthesize how the AW cooling evolved over the last century, in relation to the Arctic sea ice cover. In the mean 60% of the heat loss to the atmosphere occurred in the Nordic Seas, 30% in the Barents Sea, and only 10% in the Arctic Seas further north. The Arctic sea ice decrease over the last 100 years created more open water and permitted stronger ocean heat transfer to the Arctic atmosphere. The ocean volume and heat transport also increased, consistent with increased heat loss, and increased wind forcing. Ocean temperatures have generally increased in many areas during the last 50 years, and on Greenland this drove retreat of marine terminating glaciers. Variability in ocean heat loss to the atmosphere was primarily driven by Cold Air Outbreaks and cyclones in the Nordic and Barents Seas, and explain variability in Arctic Ocean CO_2 uptake, being ~8% of the global uptake.

1 Introduction and focus

The Arctic Seas lose heat to the atmosphere in the annual mean. The actual heat flux is only measured in short periods over a limited area and varies over time and region in profound ways. The heat loss and associated Atlantic Water (AW) circulation have been much studied due to their important consequences for each regional sea, the Arctic as a whole, climate, and the Global Ocean circulation. The main goal of this paper is to quantify and describe this heat loss, why it has increased over the last century, and how it relates to, e.g., sea ice cover, CO_2-uptake and atmospheric circulation, as well as the general warming trend from climate change. While it has been known for more than 100 years that Atlantic Water is the primary heat source for the Arctic Ocean (Helland-Hansen and Nansen, 1909), much of the variability, trends and related consequences are still undetermined.

A most important consequence of ocean heat loss is that when sea water cools, it becomes denser. The heat loss in the Arctic Seas is thus the primary driver of the transformation of the warm inflowing water into dense water that fills the North Atlantic at depth (Chafik & Rossby, 2019; Gebbie and Huybers 2011). The CO_2 solubility also increases as the waters get colder, resulting in more CO_2 uptake (Jeansson, et al.,2011). If the water column is strongly stratified, or the surface water sufficiently fresh, cooling leads to sea ice formation, which dramatically changes energy, momentum and biogeochemistry fluxes between the ocean and the atmosphere. So the heat loss dictates variability in the Arctic sea ice cover too, but it also works the other way with sea ice regulating the heat loss. If less heat is lost to the atmosphere, the heat remaining in the ocean can result in increased melting of marine-terminating glaciers with potential implications for ice discharge from the Greenland Ice Sheet (e.g. Lindeman et al.,2020; Mouginot et al.,2015). Finally, the heat loss itself is driven by atmospheric conditions, which are clearly modulated by the changing winds over the different seas (Simonsen & Haugan, 1996). We hereafter use the term 'heat loss' for the spatially integrated surface heat flux over a region like the Nordic Seas in TW (terawatt = 10^{12} W), and use the term 'heat flux' meaning the specific value at the surface for a smaller area or an observation in the unit W/m² (Table 1).

Our region of interest is the interconnected ocean north of the Bering Strait and the Greenland-Scotland Ridge (GSR), the Arctic gateways to the Pacific and Atlantic oceans, respectively. We prefer to term this collection of seas the Arctic Ocean (Fig. 1), which is consistent with the official Arctic Ocean definition of the International Hydrographic Office (IHO 1953; Jakobsson

& Macnab, 2006). We divide the Arctic Ocean into three regional seas that have fundamental different behaviour when it comes to heat loss and ocean transport; the Nordic Seas, the Barents Sea and the remaining area termed the Polar Sea (Hopkins, 1991). The Nordic Seas include the Greenland, Iceland and Norwegian Seas, and the Polar Sea covers the Beaufort, Chukchi, East Siberian, Laptev and Kara Seas, as well as the two main deep Arctic basins (Canadian and European basin, Fig. 1). We thus exclude the Baffin and Hudson Bays west of Greenland as they are not well connected with the remaining Arctic Seas (Hopkins, 1991). The name 'Arctic Mediterranean' has also been used for what we term the Arctic Ocean here, especially in oceanographic literature, starting with Sverdrup et al. (1942).

The Arctic Ocean acts like a double estuary, with AW as the main inflow and two outflows: fresh Polar Water (PW) at the surface and dense Overflow Water (OW) in the deep (Eldevik & Nilsen, 2013). Observations of the AW inflow estimate a transport of 8.0 ±0.7 Sv across the GSR (between 1993 and 2017; Østerhus et al.,2019; Tsubouchi et al.,2020). The two secondary inflows are relatively minor, bringing 0.8 Sv through the Bering Strait (Woodgate et al.,2006), and ~0.1 Sv from river runoff (Carmack et al.,2016). The total inflow is balanced by a net southward flow of PW through the Canadian Archipelago, and the southward flow of both PW and OW across the GSR. A recent estimate (1993-2016) indicates 2.7 Sv outflow of PW and 5.6 Sv of OW (Tsubouchi et al.,2020).

As will be shown, one of our main findings is that the Arctic Ocean heat loss and the Ocean Heat Transport (OHT) into the Arctic Ocean were smaller in the early part of the last century than in recent decades. The following increase in heat loss to the atmosphere has occurred in parallel with the overall warming trend and loss of Arctic sea ice. What has caused the heat loss and transport to increase, and what are the consequences? Our focus here is to review current knowledge of the variability and influences of AW inflow and – guided by a century-scale model simulation corroborated by observations – synthesize how and to what extent the inflow - in trend and variability from 1900 to present - influences 1) Arctic sea ice cover; 2) Greenland Glaciers; 3) Arctic CO_2 uptake; and 4) deep and intermediate water properties (ocean heat content).

To determine these possible influences, we need to establish the relevant long-term means and trends, and then investigate the physical mechanisms contributing to the simulated and observed changes. We start with a compact review of relevant present-day conditions in Section 2. Realizing we need to examine the variability over the last century in a consistent way, we next describe the methods used to do this (Section 3). Naturally, observational coverage has increased over time, and only a few time-series go back to the early 1900s, so simulations must be used the further back one goes. Section 4 presents our new estimates of the centennial mean values (1900–2000), before we dive into the variability and trends over time. The new results are discussed in Section 5 in light of the present-day conditions (Section 2). We conclude on the implications of the Arctic Ocean heat loss variability in Section 6 and speculate about present trends persisting into the future.

2 Review of present relevant conditions

Over the last 100 years estimates of ocean heat loss to the atmosphere in our region have evolved substantially. Due to the early Arctic explorer-oceanographers and a long history of fishery-related surveys, there are some century-long observational record documenting water mass change. Mosby (1962) presented the mean hydrographic properties, volume and heat budgets of the regional seas based on observations onwards from the Maud Expedition (1918-1925). Many estimates were close to present values, and the AW inflow was clearly identified as the largest heat source. However, as we will present here, the AW inflow volume estimate of 3.6 Sv across the GSR was probably about half of the correct value, and the 90 TW heat loss of the Polar Sea much too high (Mosby 1962). Bjerknes (1964) documented the existence of large year to year fluctuations in the North Atlantic and Nordic Seas temperature related to radiation, air-sea heat heat fluxes and OHT. Bjerknes (1964) generally found that the atmosphere forces the ocean circulation, but also the ocean temperatures influence the thermodynamics of the atmosphere. The atmospheric forcing is commonly divided into surface cooling and wind stress, indeed found to be the two main drivers of AW inflow and water mass transformation today (Timmermanns & Marshall 2020).

2.1 Atmosphere

A considerable fraction of the ocean heat loss variability is thus directly induced by the atmosphere. The total northward energy transport of the climate system across 60°N is dominated by the atmosphere, which transports approximately ~2500 TW compared to ~500 TW by the ocean (Trenberth & Fasullo 2017, Trenberth et al.,2019). Atmospheric eddies, such as cyclones and planetary waves, are key for accomplishing this transport at high latitudes both in terms of sensible heat and latent heat or moisture (Peixoto & Oort 1992, Overland et al., 1996, Graversen & Burtu 2016). The atmospheric heat transport into the Arctic peaks during winter (November through March, Fan et al., 2015, Mayer et al., 2019) and shows large interannual variations, reflecting the large internal variability of the atmosphere.

Atmospheric variability can be characterized by, e.g., EOF decomposition, into dominant spatial patterns based on sea level pressure, geopotential height, or winds. These patterns can be interpreted as large-scale circulation modes or teleconnection patterns. In the North Atlantic sector, the primary pattern is the North Atlantic Oscillation (NAO), which is well correlated with latitudinal shifting of the jet stream (Hurrell, 1995; Woollings et al., 2010), but only weakly related to atmospheric heat transport at high latitudes (Ruggieri et al., 2020). The second pattern of variability is known as the East Atlantic (EA) pattern (Barnston and Livezey 1987) and characterizes synoptic-scale pressure variations in the central North Atlantic (Trigo et al., 2008). The third pattern is the Scandinavian (SCA) pattern. The SCA represents variations in the occurrence of anticyclones over Scandinavia (Trigo et al., 2008), and favours poleward atmospheric heat transport in the Nordic Seas with a high pressure over Scandinavia (Ruggieri et al., 2020). These three variability patterns have proved useful for describing the occurrence of weather events in the Atlantic sector (Nordic and Barents Seas). They can also be interpreted as the variation of the position of the North Atlantic jet stream and storm tracks (Bueh & Nakamura 2007; Seierstad et al. 2007; Wettstein & Wallace 2010; Woollings 2010), and link short-lived weather events to monthly and longer-scale variability (Cassou et al., 2004; Michel et al., 2012).

On their way poleward, storms interact with the ocean, exchanging heat and moisture. In the Nordic Seas and the Atlantic sector of the Arctic Ocean, a large fraction of the ocean heat loss occurs in short bursts associated with the occurrence of Cold-Air Outbreaks (CAOs, Papritz & Spengler, 2017) or polar lows (Condron & Renfrew, 2013). All of these weather events, but in particular cold-air outbreaks, are often linked to extratropical cyclones (Kolstad et al., 2009, Fletcher et al., 2016, Papritz 2017).

2.2 Cryosphere

Arctic sea ice loss is now apparent throughout the year, but the amount of loss varies depending on season and region (Onarheim et al. 2018). Diminishing sea ice has a number of important consequences for marine ecology and navigation (Meier et al., 2014, Stocker et al., 2020, Lannuzel et al., 2020), plays a part in Arctic Amplification (Pithan & Mauritsen, 2014), and, by decreasing surface albedo, acts as a positive feed-back on global warming (Pistone et al., 2019). To first order, there is a nearly linear relationship between the global atmospheric CO_2 concentration, increased long-wave radiation and Arctic sea-ice extent (Notz & Stroeve, 2016) appearing in both observations and coupled climate simulations. During late spring, summer and early fall the largest ice loss is found inside the Polar Sea causing a profound change in surface fluxes there (Perovich et al., 2007). The additional solar heating of the ocean during this time of year is lost to the atmosphere during sea ice formation in the cold seasons, resulting in a small net change in the annual mean heat fluxes. This is different for the regions experiencing reduced winter sea ice , which up to now has mostly occurred in the Greenland and Barents Seas (Onarheim et al., 2018).

Large changes in annual mean heat loss in the regions experiencing reduced winter sea ice may be expected – both for trends and inter-annual variability. A clear relationship between OHT and sea ice cover variability has been established for the Barents Sea (Årthun et al., 2012, Smedsrud et al., 2013, Muilwijk et al., 2019). Here an increased AW inflow leads to reduced winter sea ice cover, stronger ocean heat loss, and increased production of dense water. There is evidence that a similar mechanism is now at play north of Svalbard, in the Polar Sea (Polyakov et al., 2017; Pérez-Hernández et al., 2019). Increased AW inflow leads to less sea ice cover also in the western Nordic Seas in climate simulations (Årthun & Eldevik 2016). This link is also found in observations covering the last decades (Selyuzhenok et al., 2020). As a result, the East Greenland Current flowing southward along the Greenland slope is now partially exposed to the atmosphere in winter so that water mass transformation directly within the boundary current may occur (Våge et al., 2018). These new areas of open water allow for more heat loss and more dense-water formation, and may thus alter the properties and composition of the OW at depth. However, while loss of winter sea ice may cool the ocean more locally, it also stops brine from being released during ice growth – so the overall and net effect on dense-water formation is not obvious, and depends on stratification often reflected in winter Seas Surface Salinity (SSS).

Northeastern Greenland forms the western boundary of the Nordic Seas. Numerous tidewater glaciers here are in contact with the ocean in narrow fjords that connect to the continental shelf (Straneo at al., 2012). These marine-terminating glaciers deliver both liquid freshwater and icebergs into the ocean. In the northeast region of the Greenland Ice Sheet, the annual flux of ice into the ocean is estimated to be approximately 35 x 10^{12} kg (Mouginot et al., 2019), equivalent to around 1 mSv of freshwater. This ice either melts near the glacier calving front (including underneath any remaining ice shelf) or as icebergs close to the coast. The bulk of the heat needed to melt this ice is supplied by the Nordic Seas. Based on the above annual ice flux (Mouginot et al., 2019) and the latent heat of melting to convert the ice-flux to energy, an estimate of the ocean heat needed is less than 1 TW per year. This is small relative to the overall cooling of the AW within the Nordic Seas. To obtain the total freshwater input from Greenland, this ice discharge has to be added to the liquid freshwater discharge from net surface melt.

Over the 1960-1990 period, the total (liquid plus solid) freshwater discharge from Greenland into the Nordic Seas has been estimated to be 107±8 km^3/yr (~3.3 mSv) (Bamber et al., 2012). In recent years (2007-2016), this has increased by approximately 24 km^3 /yr (i.e., an additional 0.8 mSv each year; Bamber et al., 2018). It remains an active area of research to assess the potential impact of this freshwater on shelf and large-scale ocean dynamics (e.g., Gillard et al., 2016). Greenland's tidewater glaciers also respond dynamically to the ocean through melting of their calving fronts and floating ice shelves. In recent decades, ocean warming has been implicated in the widespread retreat and increased sea level contribution of Greenland's tidewater glaciers (Straneo & Heimbach, 2013). In northeast Greenland specifically, variability in AW properties is understood to control melting of Greenland's largest remaining ice shelf at 79 °N (Wilson & Straneo, 2015; Schaffer et al., 2020) and has been implicated in the recent collapse of the adjacent ice shelf at Zachariae Isstrom (Mouginot et al., 2015). Quantifying past variability in the Nordic Seas thus provides essential context for understanding northeast Greenland ice sheet dynamics.

2.3 Ocean

The Arctic Ocean can largely be viewed as an enclosed basin – the Arctic Mediterranean (Eldevik, T. & Nilsen, 2013) – with the GSR as the gateway to the Atlantic in the south (Fig. 1). The atmospheric forcing is instrumental in driving the mean circulation in two ways. Firstly, heat loss to the atmosphere cools the AW inflow within the enclosed Arctic Ocean and densifies the water as it progresses northward on the eastern side in the boundary current system (Mauritzen et al., 1996; Eldevik et al., 2009). Secondly, wind stress on the surface of the Arctic Ocean, drives the mean cyclonic circulation (Nøst & Isachsen, 2013; Timmermans & Marshall, 2020) as well as circulation variability. For example, wind forcing influences the short-term variability across the GSR (Nilsen et al, 2003; Bringedal et al, 2018). On longer timescales, Dickson et al. (2000) summarized the effect of an increasingly positive phase of the North Atlantic Oscillation (NAO) and a related AW inflow increase from 1965-1996. In the real world, and in climate model simulations, wind forcing and heat loss combine to drive the full variability of the flow and water mass transformations in the region.

Our understanding of the cooling of AW as it circulates the Arctic Ocean has improved over the last decades. Using re-analysis of the atmosphere, Simonsen & Haugan (1996) highlighted the Barents Sea as an area of effective heat loss to the atmosphere (42-162 TW) in addition to the Nordic Seas (220–250 TW), but also documented large uncertainties in the parameterizations used to determine the surface fluxes. There has been quite limited efforts on how the heat loss has developed over decades. Dickson et al. (2000) found some downstream consequences of increased AW inflow in terms of sea ice loss and increased ocean temperature. Mork et al. (2014) found a Nordic Seas warming of 0.3 W/m² since 1950, and argued that air-sea heat fluxes explained about half of the interannual variability in ocean heat content in the Atlantic domain of the Nordic Seas. This was supported by Muilwijk et al. (2018), who further showed that the heat fluxes effectively damp OHT anomalies and that the wind-forced AW heat inflow anomalies do appear to change in relationship with the NAO, especially in the 1930s. Yashayaev & Seidov (2015) summarized AW variability after 1950 based on observed hydrography in the Nordic and Barents Seas, and found that AW fluctuations dominate on decadal and longer time scales. Yashayaev & Seidov (2015)found consistent correlations between the NAO and the Atlantic Multidecadal Oscillation (AMO), with low AMO values forced by high NAO and the related high heat loss in the Labrador Sea, and the AW temperature and salinity signals lagged along the inflow in the Nordic Seas. Asbjørnsen et al. (2019) documented that the AW inflow is the primary contributor to heat content variability within the Nordic Seas after the 1990s, and highlighted the possibility for related long-term predictions. Despite well-documented spatial and temporal variations, an overview of 20th century variability in relation to ongoing global warming is not established. New relevant results will therefore be presented in section 4.

A central question for the regional dynamics and thermodynamics is the relationship between the cooling of the Arctic Ocean, and the mass, heat and fresh water flows in the region. Spall (2004) presented an analytical solution based on an idealised circular basin with sloping bottom, resembling the real Arctic Ocean with the main inflow across the GSR (Fig. 1) - forced by heat loss only. He found that in the absence of topographical or far-field (AW inflow) temperature changes, the overturning, inflow volume and heat transport all scale with the overall mean heat flux Q at the surface. The Arctic Ocean heat flux is on the order 15 W/m² (Table 1), yielding a heat loss of about 200 TW over the total area of 12.3 mill km² (Fig. 2, Table 1).

The inflow volume across the GSR can be directly expressed using the mean velocity V_{in} over the $H_{in} = 500$ m deep sill and the $L = 105$ km wide slope. We generally expect an increase in OHT with more heat loss over the Arctic Ocean, and Spall (2004) finds that the inflow (in m^3/s) can be expressed as

Eq (1) $$V_{in} * L * H_{in} = \frac{H_{in}}{\rho_0}\sqrt{\frac{R\,L\,\alpha\,g\,Q}{2\,f\,c_p\,c}}.$$

Here R is the Arctic Ocean radius, f the Coriolis parameter, α the thermal expansion coefficient, c_p the specific heat capacity, g gravitational acceleration, c an empirical eddy mixing efficiency and ρ_0 a mean density. Because the slope and the sill depth, together with the other parameters, are constant in time, the inflow volume and speed are solely dependent on the density in the basin, through the thermal wind relationship and governed by Q. Representative values for the Arctic Ocean are a radius $R = 2000$ km, and a Coriolis parameter f for 80°N. Physical constants are the thermal expansion coefficient $\alpha = 0.2\ kg/(m^3 °C)$, the specific heat capacity $c_p = 3985$ $J/(kg°C)$, the gravitational acceleration $g = 9.8$ m/s^2, an empirical eddy mixing efficiency $c = 0.025$, and a mean density $\rho_0 = 1027 \frac{kg}{m^3}$. These values give an inflow of 8.5 Sv. Increasing Q from 10 W/m² to 20 W/m², equivalent to a change in integrated heat loss from 125 TW to 250 TW, increases the AW inflow with +3 Sv to 11.5 Sv (Eq. 1). A similar dependency between AW inflow and mean heat loss results from the analytical diagnostic by Eldevik & Nilsen (2013) who also accunted for the freshwater budget. In their solution an increased heatflux of 10 W/m² compares to +4 Sv of increased AW inflow.

The AW inflow is gradually cooled and densified as it progresses northward with the rim current system in the Arctic Ocean (Mauritzen et al., 1996; Eldevik et al., 2009). As the AW flows around the basin, downwelling occurs along the boundary current and much of the volume leaves the basin as OW at depth. The remaining volume exits at the surface on the western side as freshened PW. Spall (2004) concluded that in high latitude regions, and in particular in small basins, the majority of the heat is transported by the near-surface gyre circulation while deep overturning plays a smaller role. This is consistent with findings for the GSR (Li & Born 2019). The division between the horizontal gyre and vertical overturning circulation is more equal further equatorward in the subpolar North Atlantic (Böning & Bryan 1996; Lozier et al., 2019).

The AW inflow downstream of the GSR is thus a warm boundary current that cools as it travels northward (Spall 2004), but in nature it also freshens along the perimeter of the Arctic Ocean (Mauritzen 1996). Given that vertical profiles of density are available, the speed of such a boundary current V_{bc} in one location can be found following Jakhelln (1936) and Werenskiold (1935):

Eq (2) $$V_{bc} = \frac{g}{f\,\rho_{ref}} \int_{-h}^{o} \int_{-h}^{z} [\rho(-h) - \rho(z)]\; dz'\, dz$$

Here ρ_{ref} is a reference density, and the integration depth is h. Repeated CTD observations within the boundary current can be used to estimate the baroclinic transport strength as has been demonstrated for the northward AW flow across the Svinøy section just north of the GSR (Orvik et al., 2001). An AW inflow that is less dense (i.e., warmer and/or fresher) or deeper would thus lead to a stronger boundary current.

The AW inflow across the GSR may undergo a variety of transformations within the Arctic Ocean before returning south. Some AW returns southwards without undergoing much cooling, forming what is known as the AW outflow (Table 2). Rossby et al. (2018) observed ~3 Sv of AW returning south between Iceland, the Faroes and Shetland. The remaining GSR ouflow is either fresh and cold PW in the East Greenland Current, or the denser OW spilling across the ridge between Greenland and Shetland (Østerhus et al. 2019). Dense OW is transported towards the GSR along different pathways. To Denmark Strait the OW comes with the East Greenland Current (Mauritzen, 1996) and the North Icelandic Jet flowing westward along the north slope of Iceland (Jónsson & Valdimarsson 2004; Våge et al., 2011; Semper et al., 2019). The Faroe-

Shetland Channel OW has a contribution flowing southward from the Norwegian Sea (Eldevik et al. 2009; Chafik et al., 2020) and the Iceland Faroe Slope Jet arriving from the west (Semper et al., 2020). Much of the dense OW experiences the final heat loss in the interior Iceland and Greenland Seas (Swift & Aagaard 1981; Marshall & Schott 1999), with recent studies pointing more towards the Greenland Sea as the active region (Våge et al., 2015; Huang et al., 2020).

Deep convection in the Greenland Sea used to produce the coldest and densest bottom waters in the Arctic Ocean, due to the combined effect of severe winter cooling and sea ice formation (Helland-Hansen & Nansen, 1909; Aagaard et al., 1985). However, since the early 1980s only convection to intermediate depths (<2000 m) has been observed (Karstensen et al., 2005; Latarius & Quadfasel, 2016; Lauvset et al., 2018; Brakstad et al., 2019). A main reason for this change is the retreat of the sea ice edge toward Greenland (Visbeck et al., 1995). The retreating sea ice has led to reduced brine release over the central Greenland Sea since the late 1970s, and in combination with reduced atmospheric cooling this may limit the formation of intermediate water masses and OW supply (Moore et al., 2015). This has not yet occurred because a concurrent increase in salt advected in with the AW has increased upper ocean density (Glessmer et al 2015; Lauvset et al., 2018; Brakstad et al., 2019). The salt increase has resulted in enhanced ventilation of intermediate waters in the Greenland Sea since the mid 1990's (Lauvset et al., 2018). The last 10 years the trend has reversed (Mork et al., 2019), and convection in the Greenland Sea could become increasingly vulnerable to inter-annual changes in ocean heat loss.

Consistent with this study's focus on ocean heat loss, we mostly analyze the Atlantic sector of the Arctic, and explicitly leave out many of the processes and variations on the Pacific side. There are indeed wind-related changes within the Beaufort Gyre that have prominent effects on freshwater storage (Johnson et al., 2018), but there is little variability in heat loss and storage. The Beaufort Gyre is characterised by anti-cyclonic ocean circulation and sea ice drift (Timmermans & Marshall, 2020), but the heat loss is small because it is sea ice covered throughout winter (Fig. 3). For the main heat-loss region, the Nordic Seas (Fig. 1), Glessmer et al. (2015) inferred from observations and model simulations (1950–2010) that anomalous freshwater content is relatively unaffected by what is transiting from the Arctic with the East Greenland Current but rather relates to salinity anomalies arriving with the Atlantic inflow.

2.4 CO_2 Uptake

Given that the observational coverage for CO_2 in the Arctic Ocean is sparse, it is hard to quantify the present day CO_2 fluxes, and even harder to evaluate changes in time. The most recent observation-based estimate is 180 ± 130 Mt C/yr over the period 1997-2018 (Yasunaka et al., 2018). It is generally assumed that less sea ice cover will result in greater CO_2 uptake in the Arctic, both because sea ice limits gas exchange and because less sea ice leads to intensified primary production. However, some studies (e.g., Cai et al., 2010) argue that the balance between increasing pCO_2, sea ice loss, ocean warming, and biological production will prevent the Arctic CO_2 sink from becoming much stronger in the future than it is presently.

There are many processes which influence the Arctic Ocean CO_2 uptake, and there are feedbacks between all of them. The most important processes in the Arctic Ocean are the cooling of the water that increases CO_2 solubility; primary production and organic matter remineralization (Arrigo & van Dijken, 2015); biogeochemical processes during sea-ice formation and melting (Rysgaard et al., 2013); and the delivery and subsequent decomposition of organic material with river run-off, leading to CO_2 outgassing in some shelf seas (Anderson et al., 2009). There are indications of an ongoing intensification of such shelf-derived materials (Kipp et al., 2018), which may lead to changes in the Arctic Ocean carbon sink in the future. In addition, vertical mixing is an important factor because it can bring up both old water with high carbon content from organic matter remineralization and nutrients which increase primary production. Finally, physical processes such as wind speed, surface ocean turbulence, and ocean heat loss are also important for the ocean CO_2 uptake.

While all processes have an influence, the total Arctic Ocean CO_2 flux could be driven by cooling alone. The increase in Dissolved Inorganic Carbon (DIC) expected from the increased solubility as the AW cools from ~7.5 °C at the GSR to ~0.5 °C in OW is about 60 µmol/kg. Such an increase in DIC is present in available observations: Using the DIC concentrations of the inflowing AW and outflowing OW tabulated by Jeansson et al., (2011), and correcting for their anthropogenic carbon content and dilution as the salinity declines from ~35.2 (AW inflow) to ~34.9 (OW), we find a difference in DIC of 61 µmol/kg. This is not associated with a large gradient in nutrients (only ~0.1 µmol/kg in phosphate), and as such mostly reflects uptake of CO_2 from the atmosphere. Combined with a total present day throughflow of 8 Sv, this amounts to a total uptake of ~200 Mt C/yr, consistent with Yasunaka et al. (2018). The present day values based on observations are thus consistent with simple analytical scaling, but the longer term changes of the CO_2 uptake are basically unknown and therefore a primary focus in section 4.

3 Methods

NorESM simulations: Many of our new results stem from simulations with the Norwegian Earth System Model (NorESM). The main set of simulations analysed are the global ocean-ice fields of the NorESM forced by a reanalysis atmosphere from 1900-2018. The general model description is provided by Bentsen et al. (2013), while the specific forcing-setup for 1900-2009 is described in He et al. (2016). The ocean model BLOM (an extensively updated version of the Miami Isopycnic Coordinate Model, MICOM, Bleck et al., 1992) is isopycnic with 51 interior layers, referenced to a pressure at 2000 dbar, and a surface mixed layer divided into two non-isopycnic layers. The sea ice component is CICE4 (Hunke et al., 2008). A tripolar grid is used, which allows for higher spatial resolution in the high latitudes. At the equator, the grid resolution is one degree zonally and 1/4 degree meridionally. The grid gradually becomes more isotropic as latitude increases: the typical horizontal resolution in the Nordic Seas is approximately 40 km. The atmospheric forcing is mainly the 20th century atmospheric reanalysis forcing (20CRv2; Compo et al., 2011), which was adjusted by satellite observations and corrected using the Coordinated Ocean-ice Reference Experiments phase-II as described in He et al. (2016). An updated version of NorESM (NorESM2-LM, Bentsen et al., 2019) forced by the Japanese Re Analysis (JRA55-do; Tsujino et al., 2018) is available for 1958-2018 and is used for the years after 2010. These updated simulations are provided as part of the CMIP6 contribution for the OMIP2 (Ocean Model Intercomparison Project; Griffies et al., 2016) experiments. The NorESM simulations were already evaluated towards hydrography along the AW inflow path (Ilicak et al., 2016). Overall, the simulation captured the observed variability well (Muilwijk et al., 2018), with further evaluation presented here.

Atmospheric forcing: The 20CRv2 reanalysis is also analyzed directly for detecting weather events such as cyclones and CAOs. Extratropical cyclones are a key component of the atmospheric dynamics in the mid- and high latitudes, while CAOs are important for heat exchanges between the ocean and the atmosphere. We use feature detection algorithms to identify these features. Cyclones are detected as closed contours of SLP minima using the detection scheme of Wernli & Schwierz (2006). For detecting CAO events we use the definition of Papritz and Spengler (2017) and require at least a "moderate" intensity according to their classification ($\theta_{SST} - \theta_{850\,hPa} > 4$ K). We remove the linear trend and select the 15 highest and lowest years of Nordic Sea heat loss for further analysis. In a first step, we analyse the relation between ocean heat loss and the occurrence of these weather events. As a second step, we embed these feature-based results in the context of atmospheric variability patterns. We derive these variability patterns through an EOF analysis of monthly mean sea level pressure for the North Atlantic sector (90°W-40°E, 20-80°N) and the extended winter season November through April. The first three EOFs correspond to the NAO, the East Atlantic pattern and the Scandinavian pattern as expected and described in section 2.1. All analyses are performed separately for each ensemble member, and there are 56 ensemble members.

Observations, hydrography, currents and sea ice: We employ hydrographic observations from 1950 to 2019 from two different data sets. The first data set, used in Huang et al. (2020), covers the period 1980-2019 and is a collection from various archives, including the Unified Database for Arctic and Subarctic Hydrography (UDASH, Behrendt et al., 2018). The second data set, called NISE (Norwegian Iceland Seas Experiment, Nilsen et al., 2008), is a combination of data from several archives from 1900 to 2006. Due to very few observations in the first half of the 20th century, we restricted our observational analysis to 1950 onwards. Duplicates between the two databases are removed for the overlapping time period. Additionally we use available observations from the Svinøy section in the Norwegian Sea between 1996 and 2018 (NMDC, 2020), the Kola section in the Barents Sea (ICES 2020), and wind observations from the Norwegian Climate Service Centre (NCSC 2020). The simulated sea ice cover is compared to Arctic sea ice reconstructions from HadISST (Rayner et al., 2003), NSIDC (Walsh et al., 2017), and PIOMAS-20C (Schweiger et al., 2019).

CO_2 observations and new estimates: There are few observations of CO_2 and CO_2 fluxes in the Arctic Ocean, and the only available observations-based gap-filled data product covers 1997-2017 (Yasunaka et al., 2018). In addition, the NorESM simulations used in this study do not include biogeochemistry. Because we expect CO_2 fluxes to be proportional to both heat loss and sea ice loss, we overcome this challenge by using basin-wide annual averages of simulated heat loss and sea ice concentration (SIC) as predictors to extrapolate the basin-wide CO_2 fluxes back to 1900 (Table A, Sec. 2.4). Given that there is only a 12-year overlap between the observation-based CO_2 fluxes and the centennial NorESM run forced with 20CRv2, we additionally use the simulation forced by the JRA55-do reanalysis product for the period 1958-2018 to determine regression coefficients. These simulations compare well without significant biases, supporting a combination of the two. The analysis shows that CO_2 fluxes in the Nordic Seas scale with the heat flux, while in both the Barents Sea and Polar Sea the CO_2 fluxes scale with the sea ice concentration.

Greenland Ice Sheet interaction: The heat lost to melting marine-terminating glaciers and icebergs is not directly represented in NorESM in the absence of an interactive ice sheet model. The freshwater fluxes from Greenland are thus prescribed in a similar manner as Arctic rivers using mean values before 1958, and values from Bamber et al. (2018) onwards. The modest magnitude of this heat loss (~1 TW) suggests that the impact of the ice sheet on the Nordic Seas heat budget is small. Importantly, the Nordic Seas heat content impact on the ice sheet may be significant, and has been quantified. Ocean temperatures on the shelf are above 0 °C and variability in ocean temperature drives advance and retreat of marine-terminating glaciers (Straneo & Heimbach, 2013).

4 Results

We first present the baseline centennial mean values of the Arctic heat transport and air-sea exchange of heat. Then we proceed with the trends and variations following the AW flow from the Nordic Seas and onwards to the Barents and Polar Seas where it meets the sea ice. The AW has cooled towards 0 °C at this stage, but it is still sufficiently saline to yield high-density water masses that leaves the surface and eventually flows southwards back to the Atlantic Ocean across the GSR, and mostly as OW. Some of the AW has contributed to the melting of sea ice and glaciers, or it is mixed with river water becoming sufficiently fresh to exit the GSR at the surface in the East Greenland Current as fresher PW. Observations are included to the extent available, complementing and providing evaluation of the simulations.

4.1 The Centennial Means (1900 – 2000)

Surface cooling: The warm northward-flowing AW is cooled by the overlying atmosphere and the heat is transferred to the atmospheric boundary layer as sensible, latent and radiative fluxes, and ultimately radiates out to space as long-wave radiation. Because the winter-season is generally colder and longer the higher the latitude, one might expect the heat fluxes to be larger in the Polar Sea than further south. This is not the case. Heat loss from the Polar Sea is effectively restricted by the nearly permanently ice-covered sea. The Nordic Seas lose the most heat with a centennial annual mean of 115 TW (Fig. 1) based on an average surface heat flux of 45 W/m² (Table 1; all the heat loss and surface flux values presented here are annual means, unless otherwise specified). The Barents Sea has a smaller surface area and a lower surface heat flux (38 W/m²), so the centennial mean heat loss adds up to 57 TW. Furthermore, the much larger area of the Polar Sea has a surface flux of less than 2 W/m², resulting in a heat loss of only 16 TW (Fig.1).

Sea ice prevents heat loss in two ways. Firstly it forms an effective insulating layer by its low thermal conductivity. Secondly, when sea ice forms at the surface, the latent heat is released into the atmosphere, but the ocean heat loss only occurs once and where the sea ice melts. A volume flux of about 2000 km³/yr of the Polar Sea ice drifts southward through the Fram Strait into the Nordic Seas with the East Greenland Current and melts there, a process termed sea ice export, so the heat gained by the Polar Sea atmosphere during sea ice freezing actually cools the Nordic Seas. The heat transport carried by this sea ice export is estimated to approximately 17 TW, so the exported latent heat and the direct Polar Sea heat loss are comparable in magnitude. The atmosphere above the Polar Sea thus gains about 33 TW; the exported 17 TW of sea ice in addition to the 16 TW directly lost from the ocean. In the centennial mean the Nordic Seas are additionally cooled by the melting of this imported sea ice (Fig.1), adding to the heat extracted by the local Nordic atmosphere. Regionally in the Nordic Seas, the heat flux is larger in the east in the region of the warm AW inflow than in the west over the colder PW outflow (Fig. 3), consistent with warmer or more voluminous currents giving up more heat in general (Mauritzen 1996; Eldevik et al. 2009), and what, e.g., Segtnan et al. (2011) found for the 1990's.

The Nordic Seas heat loss has remained quite constant over time, with a small, insignificant long-term trend (Fig. 2, Table 1). In contrast, large increases in heat loss have occurred since 1900 in the Barents and Polar Seas. Overall the Arctic heat loss increased from 158 TW (1900-1920 mean) to 204 TW (1980-2000 mean, Fig. 2). The other heat loss trends are addressed in section 4.2.

Sea Surface Temperature (SST) and Sea Ice Concentration (SIC): The temperature of the AW inflowing across the GSR is close to 8 °C, and clearly the warmest water in the Arctic Ocean. The highest AW temperature is found at the surface in the Nordic Seas, but inside the Polar Sea the maximum is located below the fresher and colder surface layer. The two AW branches entering the Polar Sea are clearly visible in the SST (not shown) and the surface heat flux (Fig. 3) fields, with one branch flowing eastwards into the Barents Sea, and one flowing northwards west of Svalbard (West Spitsbergen Current). The only other poleward-flowing water mass is the Pacific Water in the Bering Strait, but temperatures are much lower, and the surface is sea ice covered in the centennial mean (Fig. 3). On the Pacific side the centennial mean sea ice edge is at 60°N, well south of the Bering Strait. On the Atlantic side it ranges from 60°N in the west to 80°N near Svalbard and about 70°N in the Barents Sea (Fig. 3). This enormous latitudinal range has a dynamical explanation: the unevenly distributed poleward transport of ocean and atmospheric heat.

The Ocean Heat Transport (OHT): The OHT towards the Arctic Ocean is close to that of the surface cooling, and is dominated by the AW inflow across the GSR. The centennial mean AW volume inflow across the GSR is +9.5 Sv (Fig.1, Table 2). The Pacific inflow is +0.8 Sv, and most of this leaves the Arctic Ocean through the Canadian Archipelago which has a net southward volume transport of -1.7 Sv. The volume budget is closed by the net southward transport across the GSR of -8.5 Sv. With this closed volume budget, a simulated Arctic OHT value of 179 TW is obtained (Fig. 4). This combined OHT, independent of a reference temperature, is the heat flux convergence.

Heat transport for the individual straits requires, however, a reference temperature. Because 0 °C is a representative temperature of the cold dense water flowing southward across the GSR (Fig. 5), we adopt 0°C as our reference temperature following e.g. Årthun et al., 2012 and Rossby et al., 2018. We also use the term 'heat transport' and the TW unit also for the individual strait values (Table 2). Other authors, especially those using observed values where a closed volume budget is more challenging, prefer to use the term 'temperature flux' and the 'unit' [TW - equivalents]. Referenced to 0°C the GSR heat transport is +172 TW, the Bering Strait has a transport of +0.9 TW, and there is a net positive contribution from the Canadian Archipelago of +6.6 TW (Fig. 4). About half of the heat transport across the GSR is due to the horizontal gyre (estuarine) circulation with the remainder coming from the deep overflows. Note that our analysis follows the GSR and is therefore not directly comparable to previous analyses that focus on the meridional OHT (e.g., Li & Born, 2019).

Within the Arctic Ocean the centennial mean net heat transport in the Fram Strait is northward directed with a value of +15 TW, with the largest contribution from the southward flow of water colder than 0 °C (Fig. 1 and Table 2). Taking the southward sea ice export into account (Fig. 1) brings the net ocean and sea ice transport in the Fram Strait close to zero. The centennial mean heat transport to the Barents Sea is +53 TW (Fig. 1), with the largest component in the Barents Sea Opening (Fig. 1 and Table 2). Both volume and heat transport show large variations and trends at the different sections. This variability is discussed in section 4.2. A noticeable and important overall Arctic OHT increase from roughly 150 TW (1900-1920) to 200 TW (1980-2000) should be mentioned, mostly governed by the heat transport across the GSR (Fig. 4).

Hydrography and dense water formation: The inflowing AW is transformed into denser, but also fresher water. This means that the cooling is the ultimate driver of the densification. The progressive observed cooling and freshening from AW to OW is clearly illustrated in Fig. 5. The transformation falls along a close to linear line in T-S space, showing a gradual cooling and freshening along the cyclonic flow of AW from the Faroe-Shetland Channel towards Fram Strait, and southwards again along the east coast of Greenland. By the time the OW spills across the GSR, the water has cooled by roughly 7 °C compared to the AW inflow. More than 60% of this cooling has occurred before the AW subducts beneath the fresh PW in Fram Strait, and the transformed AW is sufficiently dense to contribute to the GSR overflow. Dense water formed in the Iceland and Greenland Seas during winter additionally contribute to the OW as described in Section 2.3.

The hydrographic properties at the GSR, of both inflowing AW and outflowing OW, are quite well represented in NorESM (Fig. 5). In general, the largest bias is found in salinity. The observed and simulated Iceland Sea Intermediate Water differ by about 0.15 in salinity but matches well in temperature. We also note that the cooling of the AW as it progresses northwards appears to be a little too strong in NorESM (Ilicak et al., 2016). For the Barents Sea Opening, the simulated mean temperature is about 1.0 °C lower (Fig. 5) and salinity 0.1 lower than observed values. A probable explanation for this deficiency is that the model is too diffuse, losing the AW heat and salt too quickly through lateral mixing as it flows northwards. The transformation from a density of ~27.4 kg/m³ (inflowing AW) to ~28.0 kg/m³ (outflowing OW) is realistically captured, and simulated trends and anomalies are independent of the mean state.

The atmospheric circulation and heat loss: The surface heat flux is largest over the northward-flowing AW between the GSR and the sea ice (Fig. 3). The heat loss increases towards the north in Fram Strait west of Svalbard and in the Barents Sea. The spatial pattern of this heat loss north of 60°N is very similar between 20CRv2 and NorESM, and this is reassuring as the two have quite different sea ice cover distributions. The annual mean heat fluxes in the individual seas are somewhat different from the simulated heat loss (Fig. 2), which is mainly caused by the active ocean and sea ice components of the NorESM (not shown). The NorESM generally simulates higher Arctic sea ice concentrations in the period prior to 1950, as we will later discuss for the Barents Sea. This is also the case for the Nordic Seas and the Polar Sea.

Given the inherent uncertainties when reconstructing the atmospheric state in the Arctic based on only limited surface observations during the first half of the 20^{th} century, we do not examine trends in atmospheric heat transport. Instead, we analyze which atmospheric features drive the ocean heat loss and contributes to its large interannual variations over the regional seas (section 4.2).

CO_2 uptake: Centennial mean CO_2 uptake for the Arctic Ocean (Table 1) is calculated based on the extrapolated basin-wide CO_2 fluxes (Fig. 6). Just as for the heat loss, the Nordic Seas dominate the total Arctic Ocean CO_2 uptake, but the CO_2 uptake in the three basins become more similar with time. This is likely due to the strong influence of sea ice loss – more open water – on CO_2 uptake in the Barents and Polar Seas. The centennial mean CO_2 uptake in the Arctic

Ocean (209.9 MtC/yr, Table 1) is consistent with the back-of-the-envelope calculation presented in Section 2.4, and previous estimates (Yasunaka et al., 2018). This suggests that the heat loss is the major driver of the Arctic Ocean carbon sink and that biological drawdown plays a smaller role. The Arctic Ocean CO_2 uptake estimated here corresponds to ~8% of the global ocean CO_2 uptake of ~2500 MtC/yr (Friedlingstein et al., 2019). This is much larger than the area of 12.4 mill km² (3.4% of the total ocean area of 362 mill km²) would suggest, highlighting the importance of the Arctic Ocean as a major carbon sink during the last century.

4.2 Variability and Trends (1900 - 2000)

With the long-term means established for the Nordic, Barents and Polar Seas (Fig, 1), we continue to describe variations and trends. We do this by first presenting the overall variability in atmospheric forcing over the larger Arctic Ocean region. Our main focus, as before, is on the Nordic Seas as the major heat loss variability occurs there (Fig. 2). After that we describe the various consequences and related AW and heat variability elsewhere within the Arctic Ocean.

The atmospheric circulation and heat loss: Consistent with previous studies (e.g., Papritz & Spengler 2017), pronounced ocean heat loss over the Nordic Seas is associated with an increased frequency of CAOs (Fig. 7a). In absolute terms, the frequency of occurrence increases from 10-15% of the extended winter season for low heat flux years to 20-25% of the time for high heat flux years. Results presented here are for an extended winter for each calendar year (January-April, November and December), but results for consecutive extended winter seasons (November-April) and core months (December - February) are very similar. This highlights that our results are insensitive to the definition of winter.

CAOs over the Nordic Seas are associated with more cyclones than average over Scandinavia and the eastern part of the Nordic Seas (Fig. 7b), in accordance with Papritz & Grams (2018). This is because cyclones situated in this region have their cold sector situated over the Nordic Seas. In the cold sector, they advect cold air masses from the central Arctic and through Fram Strait over the relatively warmer ocean, yielding more CAOs (Fig. 7a). Further, the increase in cyclone activity over Scandinavia indicates a reduced frequency of Scandinavian anticyclones and blocks linked to the negative phase of the Scandinavian pattern. The relation can be quantified by the negative correlation between a Scandinavian pattern index time series and the ocean heat loss of r = -0.48 (not shown).

While the Nordic Seas heat loss is related to more cyclones over Scandinavia, it is also related to fewer cyclones between Greenland and Iceland (Fig. 7b). The reduction in cyclone occurrence here of ~7% represents about one-fourth of the climatology (30%, blue contours). Accordingly, the heat loss is correlated with the East Atlantic pattern (r = -0.49), which in its negative phase is associated with fewer cyclones over and to the west of the British Isles. The ocean heat loss in the Nordic Seas exhibits a negative correlation also with the NAO, but it is comparatively weak (r = -0.15) and not statistically significant.

Ocean Heat Transport: The OHT of AW across the GSR has varied due to changes in volume transport and temperature over the last century. The primary reason for the steady increase in OHT from +150 TW to +200 TW over the last century (Fig. 4) is an enhanced flow across the GSR of about +1 Sv, which on the outflow side is split into OW and PW in equal parts (Fig. 8). The enhanced volume transport alone explains a linear trend of 28 TW/century while changes in temperature on their own would cause an increase of 17 TW/century. Both the overturning and gyre components contribute about equally to the increase as expected from the similar trends in OW and PW volume transports. No significant trends in volume transport are found for the Canadian Archipelago and the Bering Strait over the last century (not shown). The cause of this volume transport increase across the GSR is attributed to Arctic Ocean heat loss and local wind forcing as discussed in section 5. Both the OW and the PW have cooled slightly over the last century, but appear to stabilize or warm in recent decades (Fig. 8). For the AW returning south across the GSR, the AW outflow, there has been no trend in volume, but a general small long-term warming.

Nordic Seas heat loss: The Nordic Seas heat loss has remained quite constant (Fig. 2) despite a large increase in poleward OHT across GSR, and a loss of Nordic Seas ice cover. The long-term heat loss trend of +6.2 TW/century (Table 1) is only +5% of the total heat loss and thus quite small. This implies that the Nordic Seas have warmed or that heat now reaches further poleward. Consistently, the increased GSR OHT mostly continue into the Barents Sea with the retreating sea ice. There is also a small negative contribution from the Fram Strait, with more cold water flowing south in time. Furthermore, there has been a systematic warming in the simulated Nordic Seas since the 1970's of about +0.5°C (volumetric mean, not shown). This warming is also consistent with the small reduction in the Nordic Seas heat loss to the atmosphere of about 10 TW over the same time (Fig. 2).

The (annual mean) Nordic Seas ice cover dropped from ~700.000 km² around 1900 to ~500.000 km² in the late 1970's. The sea ice cover has been quite stable since the 1980's with values in the range 400.000 to 450.000 km². The main reason for the sea ice decrease is not related to heat loss - as the heat loss has remained fairly stable (Fig. 2). The annual changes of Nordic Seas heat loss are also unrelated to the sea ice area (r = -0.09), they are rather explained by variations in the atmospheric circulation as described above. This is consistent with most of the heat loss occuring away from the sea-ice covered areas, over the warm AW in the east (Fig. 3). There is only a small correlation between sea ice area and the net OHT (r = -0.27), but there is a much larger correlation between sea ice area and the inflowing OHT across the GSR (r = 0.77). This means that the OHT in the Fram Strait and the Barents Sea Opening are unrelated to the Nordic Sea ice cover, as one might expect. The GSR OHT seems to drive a similar response for Nordic Sea ice as documented in the Barents Sea with 10 TW of OHT leading to an ice loss of 70.000 km² (Årthun et al., 2012) **(**Presently not shown – available as supplementary Fig. Z). Reduced sea ice import from the Polar Sea has also contributed to the Nordic Seas ice loss. Over the 1920-1950 period this import was as high as ~3000 km³/yr, largely caused by a thicker sea ice cover. The ice import dropped to ~2000 km³/yr towards 2000, and the correlation between sea ice import and the Nordic Sea ice area is r = 0.55. This decreased import of ice represents a drop in required heat for melting from 20 to 12 TW, a magnitude well within range of annual variability of ±20 TW (not shown).

Barents Sea heat loss has increased steadily over time (Fig. 2), with a very systematic congruent increase in OHT and decrease in sea ice cover (Fig. 9b). The increased heat loss corresponds to an increase in the area-averaged surface heat flux from ~30 W/m² around 1900 to ~50 W/m² around 2000. This is first and foremost a consequence of sea ice retreat, as there is a high correlation between Barents Sea open water area and heat loss (r = 0.86). Using a representative heat flux of the open water area (Fig. 3) of 100 W/m², most of the increased cooling (+30 TW between 1900 and 2000, Fig. 2) can be explained by the more extensive open water area (sea ice area of ~750.000 km² in 1900 decreasing to ~450.000 km² in 2000, Fig. 9). This further supports earlier findings (Årthun et al., 2012; Smedsrud et al., 2013) concluding that the OHT is the main driver of sea ice and heat flux variability in the Barents Sea, with positive OHT anomalies preventing sea ice formation and letting the heat escape to the atmosphere; "The Barents Sea Cooler" (Skagseth et al., 2020). Consistent with Muilwijk et al. (2018), most of the increased

Barents OHT is related to an increase in volume transport of about +1 Sv over the last century (not shown). These changes occur at the same time as there are large observed changes in ocean temperature at the Kola section (Fig. 9a). The NorESM simulations capture this ice-ocean variability well although the mean temperature is too low.

Polar Sea heat loss also increases steadily over time. The cooling tripled from about 7 TW in 1900 to around 21 TW in 2000. The annual mean heat loss remains below 3 W/m², mostly explained by long-lasting sea-ice cover and net sea ice growth. Open water area increased from around 5% in the early period (1900-1920) to 20% after the 1990's; this corresponds to a loss of about 1 mill km² of sea ice area. In the annual mean this sea ice loss is occurring directly north of the land areas from Svalbard, along Siberia to Alaska (not shown). There is a small net increase in OHT for Bering Strait and the Canadian Archipelago (Fig. 4), as well as for exports through the Fram Strait and the Barents Sea (not shown). The northward flow is warmer than 0°C in all straits apart from the Barents Sea exit, so the increased flow there offsets the increased transport in the other straits and explains the relatively low OHT transport of ~4 TW in 1900-1920, increasing to ~16 TW in 1980-2000.

Hydrography and dense water formation: The net AW-inflow increase across the GSR of about 1 Sv over the last century was compensated by an equally large increase in the southward outflow. Approximately 0.4 Sv of this increase can be assigned to the OW (Fig. 8), mainly to the OW spilling across the GSR in the Faroe Shetland Channel (not shown). The southward transport of cold low salinity PW in Denmark Strait has increased by 0.6 Sv, while no significant trend was found in the AW outflow (Fig. 8, Table 2). The simulated positive trend in OW volume transport occurred together with a simulated negative trend in OW temperature until the 1980's that is comparable to observations after 1950 (Fig. 5, 8 and Q). Systematic cooling was evident also in the simulated upstream intermediate waters during the same period (not shown). The largest temperature decrease (of 1°C and 0.5°C for the Iceland and Greenland seas intermediate water, respectively) occurred between 1920 and 1960. This is consistent with the large increase in atmospheric heat loss over the same time period (Fig. 2). After the 1980's, the intermediate water masses started to warm (Fig. Q). This occurred concurrently with both increased AW inflow temperature and reduced atmospheric heat loss. A small, but persistent warming has occurred also in the OW after around 2000.

Greenland Ice Sheet melting: Variability in ocean temperature adjacent to the Greenland ice sheet is understood to drive advance and retreat of marine-terminating glaciers (e.g. Straneo & Heimbach, 2013). Slater et al. (2019) developed a parameterization relating tidewater glacier terminus position to ocean temperature on the continental shelf and to the subglacial discharge of surface melt. Application of this parameterization to NE Greenland allows us to quantify the impact of ocean variability on the regional ice sheet over the past century.

The parameterization suggests there have been sustained periods of both advance and retreat over the past century (Fig. 10). According to the proposed parameterization, sustained retreat occurred during 1900-1925 (Fig. 10b) during a period of increasing subglacial discharge but stable ocean temperature (Fig. 10a). This is followed by ~50 years of advance during a period of cooler ocean temperature and reduced subglacial discharge. From 1980 to present a sustained retreat is projected in response to both ocean warming and increased subglacial discharge. The response of glaciers to the ocean alone (Fig. 10b, blue) can be isolated by applying the parameterization while holding subglacial discharge constant (Slater et al., 2019). Based on these results, the ocean variability alone explains a significant proportion of marine-terminating glacier advance and retreat in NE Greenland over the past century.

Observations of tidewater glacier terminus position from satellite imagery since 1984 (King et al., 2020) also show sustained retreat during this period and agree well with the projections (Fig. 10b). The longer term projected trends are also very consistent with terminus position changes observed in south-east Greenland since 1931 based on historical and satellite imagery (Bjørk et al., 2012).

CO_2 uptake: The calculated CO_2 fluxes from 1900-2009 (Fig. 6) show a rather stable uptake in the Nordic Seas, with no discernible trend. This is consistent with the small (not significant) trend in heat loss over the Nordic Seas in this time period (Fig. 2). However, the gradual sea ice loss results in essentially a doubling of the ocean CO_2 uptake (fluxes) in both the Barents and Polar Seas. In the Barents Sea the mean CO_2 flux increased from -7 to -12 mmol/(m^2 d) over the 20th century, while the mean Polar Sea CO_2 flux increased from -1 to -2 mmol/(m^2 d), according to these, admittedly simple, extrapolations. The much smaller Barents Sea has a larger overall uptake, reflecting both the larger areas of open water and the strong cooling, but the total uptake is similar between Barents Sea and Polar Sea from 1960-2000 (Fig. 6).

4.3 The new normal (2000 - 2018)

Atlantic Water Inflow volume: There are no observed trends in AW inflow volume across the Svinøy section west of Norway between 1996 and 2018. This is nicely captured by the NorESM model (Fig. 11 b). The observed variability of the AW inflow in the eastern branch at the Svinøy section is presented in Fig. 11 b) and is ±0.5 Sv in the last 20 years. There is a low positive correlation with the local wind forcing. The baroclinic transport of the western branch at the Svinøy section was calculated based on Eq (2) with Coriolis parameter f for 60°N, reference density $\rho_{ref} = 1027.5\ kg/m^3$, integrating to a depth h=500 m. The resulting mean mean baroclinic AW inflow value was calculated from 123 CTD casts taken at one single location offshore of the slope current between 1996 and 2018. This mean baroclinic AW inflow is 4.1Sv ±0.1 Sv and was added to the observed AW volume of the inner branch in Fig. 11 b). The de-seasoned standard deviation of the western branch baroclinic transport is 0.9 Sv and is likely mostly due to eddy variability.

The halting Barents Sea Cooling Machine: New observations clearly indicate a major change in the Barents Sea over the last 20 years. Fig. 9 shows a continued loss of annual sea ice cover, and a continued warming. The sea ice loss has mostly occurred in the north-east, and in this region there has also been an increased heat loss (Skagseth et. al 2020). In the south-west, however, heat loss was substantially reduced in the 2000s, compared to the 1980s and 1990s, to the extent that total Barents Sea heat loss decreased in the recent decades (Fig. 2). This has created a warming of the dense water that exits to the Polar Sea via the St. Anna Trough (Fig. 1). The major change is an increase in sensible heat flux over the southern Barents Sea, while there were minor changes in both latent, shortwave and long-wave surface fluxes, based on the ERA-interim re-analysis (Skagseth et al., 2020). Asbjørnsen et al. (2020) shows that most of the recent change is caused by high AW OHT and reduced surface heat loss.

Hydrography and dense water formation: Since the 1980's there has been a persistent warming in the interior Iceland and Greenland seas with a rapid increase of 0.5°C and 0.7°C from 2000 to 2018, respectively (Not shown – available as supplementary Fig. Q). The long-term (1950-2019) trends for the OW are still showing cooling (Fig. 5), but there is a small sign of observed OW warming after 2000 that is partly simulated by the NorESM. One main reason for this warming is the increased temperature of the AW inflow. Lauvset et al., (2018) found a strong correlation (r=0.72) between the AW temperature in the Faroe Shetland Channel and the near surface temperature in the central Greenland Sea 3 years later. A similar correlation (r=0.80) was found for salinity, which suggests that AW anomalies transfers into the Greenland Sea through lateral mixing (Eldevik et al., 2009), although direct advection could also take place. The other main reason for the observed intermediate water warming is a reduced wintertime heat loss. Moore et al., (2015) showed that the magnitude of the winter heat loss in the central Iceland and Greenland Seas has declined by 20% since 1979, mainly because the ice edge and the cold winds are further away. There are thus different rates of warming in the atmosphere and ocean that at present may affect the Greenland Ice sheet.

Greenland ice sheet: Simulated subsurface ocean temperature on the NE Greenland continental shelf has increased consistently since approximately 1980, but a particularly rapid increase of >0.75°C occurs between 2000 and 2017 (Fig. 10 a). The simulated subsurface ocean temperature exceeded +1°C in 2017 for the first time in over a century, and the mean temperature post 2000, at 0.63°C, is higher than during any 20-year period since 1900. The tidewater glacier response has been a sustained retreat (Fig. 10 b), with a particularly rapid retreat of 0.48 km post-2000. Even if ocean temperatures now stabilize, tidewater glaciers in NE Greenland may continue to retreat due to the long response time of tidewater glaciers to climate forcing. As such, in the absence of ocean temperatures returning to pre-2000 values, tidewater glaciers in NE Greenland are likely to remain in a retreated or further retreated state over the next decades.

The Arctic sea ice loss and CO_2 impact. The gap-filled data product for Arctic Ocean CO_2 fluxes over the period 1997-2018 (Yasunaka et al., 2018) shows no significant trend in the Polar Sea CO_2 fluxes. However, in the Nordic Seas and the northern Barents Sea these estimates show that CO_2 uptake has strengthened. Interestingly the fluxes have weakened in the southern part of the Barents Sea, consistent with the local observed warming and smaller heat loss (Skagseth et al., 2020). While both the Nordic Seas and Barents Sea exhibit stronger CO_2 uptake, the mechanisms are different. In the Barents Sea the increased CO_2 uptake is primarily a consequence of the sea ice loss (Fig. 9), and the present uptake has increased from the ~59 MtC/yr estimated in Smedsrud et al (2013) to about 80 MtC/yr today (Fig. 6). In the Nordic Seas the increasing CO_2 uptake is instead due to increasing disequilibrium between pCO_2 in the atmosphere and in the mixed layer. In the Polar Sea, impacts of the retreating sea-ice edge on the CO_2 flux is evident in all regions that have lost ice the past few decades. There are in general strong correlation between CO_2 uptake and number of ice free days, and this pattern is expected to spread northwards as the ice retreats further.

5 Discussion

Our review and analysis presented three main results over the last century; 1) The sea ice cover on Arctic Seas is shrinking and there is a related increase in heat loss and Ocean Heat Transport (OHT) for the Barents and Polar Seas. 2) The Nordic Seas dominate heat loss in magnitude and carried by AW, but the variability is directly driven by the atmosphere. 3) The are related consequences with warming shelf waters affecting melting of glaciers on Greenland and the increased heat loss affecting Arctic Ocean CO_2 uptake and production of dense water flowing southwards towards the North Atlantic across the GSR. A simplified summarizing sketch of the main dominating processes is offered at the end. We start by discussing the regional contrasts in the strongly coupled heat loss, OHT and sea ice cover, before venturing into the temporal changes.

Regional Arctic heat loss: Generally, the heat flux is larger in the east than in the west, caused by the larger temperature contrast between the warm AW inflow and the cold Arctic atmosphere (Fig. 3, Mauritzen 1996; Segtnan et al., 2011). The heat loss values are largely consistent with earlier estimates stating that the Nordic Seas dominate the heat loss, but are in the lower range (Simonsen & Haugan 1996). Given that most earlier estimates are from recent decades and the large positive trends presented here - this is within expectations. The centennial mean values are however still consistent with new estimates from ocean re-analysis after 2001 (Mayer et al., 2019). These show consistent values with average heat fluxes of ~40 W/m² in the Barents Sea and values below 5 W/m² in the Polar Sea, similar to Table 1.

Temporal variability of heat loss: The overall Arctic heat loss increases over time (Fig. 2). The heat loss trends over the last century is mostly found in the Barents Sea and in the Polar Sea, reflecting the sea ice retreat and expansion of open waters there (Fig. 9). The generally increasing open water area in the Arctic Ocean thus generally allows a larger heat loss to the atmosphere, and the implied mean heat flux in the new open water area is 40 W/m² (Not shown – available as suggested supplementary Fig. X). There has also been a sea ice loss in the Nordic

Seas - but only a small (and not significant) trend in heat loss. The major explanation for the different heat-loss and sea ice relationship in the Nordic Seas is that the sea ice loss occurred in regions with cold surface water. Regardless of the small heat loss trends in the Nordic Seas, it is here where the bulk of the heat loss takes place, as already suggested by Helland-Hansen & Nansen (1909). The Nordic Seas also dominate the year-to-year variability, directly forced by the atmospheric circulation (Fig. 7). Consistent with other recent work (e.g. Papritz & Grams 2018) we find that in the years with most heat loss in the Nordic Seas more cyclones than usual occur over Scandinavia (a negative SCA pattern) and drive winter-time bursts of cold air over open water (CAOs).

Temporal variability of Arctic Sea ice cover: The NorESM sea ice loss is similar to observation-based Arctic sea ice reconstructions (Walsh et al., 2017; Brennan et al., 2020) for the time period after 1960. We focused on the Barents Sea ice cover variability (Fig. 9 b) as it is the region that mostly affects the heat loss trends. For the period before 1960 the NorESM Barents Sea ice cover has similar variability, but overall larger values. These annual values are mostly reflecting the winter sea ice, as there is not much summer sea ice in the Barents Sea (Onarheim et al., 2018). The observational coverage in winter is also relatively scarce prior to the 1960's (Walsh et al., 2017), and these values are at least in-part reflecting the use of low climatic mean values from recent decades. As the NorESM values reflect atmospheric forcing from the 20CRv2 that incorporate observations from available weather stations, it is not clear which of the sea ice estimates that best reflect "observations". The NorESM fields are at least energetically consistent with the simulated ocean below, but there are also unscertainties in parametrizations of surface fluxes. The decreasing Barents sea ice cover is consistent with the available atmospheric forcing, and the ocean variability appears well captured as the independent temperatures of the Kola section reflect (Fig. 9a). We also know that there is a very physical link between the AW inflow, ocean temperature and the Barents Sea ice and heat loss (Smedsrud et al., 2013). The Barents sea ice decline between 1900 and 1950 is thus consistent with the observed increasing temperatures (Fig. 9a) that provides confidence in the simulated sea ice cover. The cold bias in the model does not affect the variability and is probably caused by the relatively coarse resolution, leading to too much mixing with the colder coastal waters (Docquier et al., 2020). The simulated Barents sea ice loss is also consistent with new Arctic estimates over the last century (Schweiger et al., 2019) who found a significant decline in sea ice volume in the Atlantic sector from 1900 - 1940 related to early-twentieth century warming. Muilwijk et al., (2018) found that this early warming was more related to a warm temperature anomaly in contrast to the AW volume anomalies dominating later in the century.

Heat loss and Ocean Heat Transport: The overall Arctic heat loss variability contributes to variations in OHT over time. The analysed NorESM forced ice-ocean simulations apply both wind and buoyancy forcing to drive the inflows and outflows, so we attempt to extract the heat loss contribution using a simplified analytical Arctic Ocean model (Eq. 1, Spall 2004). Figure 11 a) shows that the heat loss explains a large portion of the variability since 1900. A close to 50% increase of the overall Arctic heat loss Q is a close match to the simulated increase onwards from 1900 (150 ⇒ 225 TW, Fig. 2 or 12 ⇒ 18 W/m², Fig. 11 a). These heat flux values lead to a surprisingly good fit with the NorESM values with an increased AW inflow from 9.5 to 11.0 Sv. An increase in the AW OHT has been found as a consequence of increased CO_2 forcing using a fully coupled climate model, and could thus be expected (van der Linden et al., 2019).

It may appear surprising that the simple relationship by Spall (2004) can explain much of the variability in a forced complex climate model like the NorESM. Given these limitations such as the assumption of a perfectly circular basin, the representativeness of this relationship is spanned out using a range of plausible values: the radius of the basin $R = [1900, 2100]$ km, slope width $L = [90, 120]$ km, thermal expansion $\alpha = [0.18, 0.22]$, eddy mixing efficiency $c = [0.22, 0.28]$, and the depth of the GSR $H = [400, 600]$m. The overall relationship between the heat loss and the overall volume inflow remains clear, and is also consistent with first order analytical diagnostic of the volume, heat and salt budget(Eldevik & Nilsen 2013). The inflow strength is goverened by the thermal wind equations and is a steady state solution. Consistently there is a better fit for the Spall (2004) line with the 5-year means than the annual values (Fig. 11 a). There is indeed some volume flow variability of order ±1Sv that is away from the expected heat loss (flux) releationship, especially on the year-to-year basis. We therefore turn to the wind-driven variability below.

As discussed above is a majority of the OHT increase over the last century explained by an increased AW volume inflow, as temperature changes were minor and the OHT across the other Arctic straits remained stable. This is consistent with new short-term results from farther south in the subpolar North Atlantic, that also find the OHT to be primarily dictated by AW inflow (Lozier et al, 2019). Recent work confirms a high OHT northwards through the Nordic Seas over the last decades. Eldevik & Nilsen (2013) estimated an Arctic Ocean heat loss of 282 TW based on observed mean inflow and outflow temperature and volume. They ignored the contributions from the Bering Strait and Canadian Archipelago, so this is broadly in line with our values after the 1990's (up to 250TW). Based on moored observations across the Arctic gateways and an inverse calculation, Tsubouchi et al., (2020) estimated an increased Arctic OHT from ~ 290 TW in the 1990's to ~310 TW in the 2000's carried by both increased AW volume and temperature. Most of this heat (281 ±24 TW) is transported across the GSR. The NorESM numbers are lower, but consistent with a new state estimate for 2002-2017 suggesting a mean OHT of 223 TW across the GSR, and a total Arctic Ocean heat loss of 239 TW (Nguyen et al 2020). Using primarily shipboard temperature and velocity measurements since 2008, Chafik & Rossby (2019) estimated a heat transport of 273 ±27 TW across the GSR. These numbers are ~50 TW higher than the comparable simulated northward OHT across the GSR (Fig. 4). So while the NorESM has inflowing AW transporting 285 TW there is also ~100 TW transported out by the -3.3 Sv of AW outflow (Table 2), making the net long-term mean OHT as low as 172 TW. About -1.6 Sv of the AW outflow occurs in the Faroe-Shetland channel (Fig. 1, further regional detail offered in supplementary Fig. K). This is twice the amount found by Berx et al.(2013) from 1994-2011, but comparable to the estimate from Rossby et al., (2018) here. The rest of the outflowing AW is distributed in the Denmark Strait and east of Shetland (supplementary Fig. K). The separation used between southward flowing AW and OW does influence the volume of outflowing AW, and some authors appear to vary this separation between the straits (Østerhus et al., 2019). We classified water denser than 1027.8 kg/m³ as OW (Fig. 8). Rossby et al., (2020) suggests that the OHT transport northwards across the GSR peaked in 2010 at ~270 TW, and predicts that it will reduce to ~210 TW in the decades ahead based on Atlantic SST variability 0-60°N (Atlantic Multidecadal Variability, Trenberth & Shea, 2006). Chafik & Rossby (2019) and Tsubouchi et al., (2020) thus both find that the overall OHT in recent decades is substantially larger than the simulated net OHT of ~200 TW (Fig. 4). Despite this disparity we may conclude that the OHT has increased over the last century and appears to have peaked temporariliy. This points to the importance of a continued monitoring of this inflow.

Wind forcing of the AW inflow variability: Several studies show a strong link between the AW inflow and the large-scale wind forcing in the region. For example, Muilwijk et al. (2019) showed a clear relationship between NAO-type wind forcing in the Greenland Sea and the AW volume transport northward. Also, Bringedal et al. (2018) analyzed AW inflow across the GSR over the instrumented period (1996-2016) and found that wind forcing drives much of the seasonality and also interannual variability, but here overturning and buoyancy forcing must also be considered as the time scale increases. For monthly time scales there is a connection to the NAO for the inflow along the Norwegian coast over these 20 years, where the along-coast wind stress drives an Ekman transport towards the coast that piles up water locally, and drives a barotropic inflow (Eq. 2. in Bringedal et al., 2018). We have tested this relationship for the 1900-2000 period and find a consistent response to the simulated GSR inflow from the along-coast wind strength (Fig. 11 b). The correlation is high in the NorESM simulations (r=0.78), but lower and not significant for our new available observations in the Svinøy section (1996 - 2018). The increasing wind forcing thus partly explains the increased volume inflow across the GSR. There is no correlation between the (annual mean) GSR wind forcing and the ocean heat loss north of the GSR, so these are independent drivers of the inflow. Orvik et al. (2001) calculated the mean value of the outer (western) branch at Svinøy based on hydrography, and found a (1995-1998) mean of 3.4 Sv. An updated baroclinic estimate of this branch is 4.14 Sv. The observed values in Fig. 11 b) shows variability of the eastern inner branch with +5.14 Sv added to represent this outer branch and the +1 Sv inflow around Iceland.

Several studies have documented an increase in wind speed in some regions of the world ocean. A small general and overall increase in surface ocean flow speed of +1 cm/(s yr) was also found for the 1992 to 2015 period (Wunsch, 2020) based on satellite sea level data. Young & Ribal (2019) documented an increase in wind speed between 1985 and 2018 of about ~2 cm/s year in the Southern Ocean, and of about 1 cm/s year in the North Atlantic. These values are comparable to the +2 m/s increase over the last 100 years in the 20CRv2 reanalysis west of Norway (Fig. 11 b). A long-term increased wind forcing for many locations in the Norwegian Sea was also documented by Vikebø et al. (2003) for 1900-2000. They also found a consistent increase in wave height in this area, but also noted a reduced wind forcing between 1880 and 1900. Wind observations were very limited before the 1950's, but we analyzed available observations from an island west of Bergen (Utsira) that is consistent with the overall increase shown in Fig. 11 b), although there are some substantial data gaps. However, wind increases are not visible in recent reanalysis (e.g. ERA5) for the last 40 years (1979-2019), and thus trends arise mainly from the early part of the century. The increase in wind speed along the Norwegian Sea, and the related wind stress forcing on the ocean can thus explain part of the observed increase in the AW inflow and the OHT transport (Fig. 4). For the future there is little consensus regarding expected changes in wind forcing, so we take this driver of OHT variability as natural climate variability. There are for example large inter-model differences in projected wind speed for the North Atlantic region, but also some consistent strengthening and squeezing of the zonal flow (Oudar et al., 2020).

Implications of Arctic heat loss, sea ice and OHT: The discussion above summarized the combined consistent relationship between the Arctic heat loss, the OHT, and the sea ice cover. Over the last century the heat loss and OHT increased, while the sea ice cover decreased. This relationship was perhaps expected based on analytical models and previous analysis, but was quantified and presented in a consistent model framework here. Clearly the inflowing AW OHT anomalies are not fully escaping to the atmosphere through cooling in the Nordic Seas, but some heat is left and continues onwards into the Barents and Polar Seas. Our main hypothesis listed in the introduction was that the inflowing OHT AW anomalies influence the; **1) Arctic sea ice cover, 2) Greenland Glaciers, 3) Arctic CO2 uptake, and 4) deep and intermediate water properties** (Fig. 12). For the Arctic sea ice cover we established that there is an expected analytical relationship between them consistent with simulations over the last century; less sea ice in itself allows a larger heat loss and accommodates a stronger OHT by the AW. Arctic sea ice loss is one of the well-established consequences of global warming and increased CO_2 levels in the atmosphere (Notz & Stroeve, 2016).

How would this ‘heat-loss\sea-ice\OHT’ relationship have played out in the absence of global warming? As natural climate variability is strong in the Arctic - Atlantic sector we speculate that the wind forcing would then have dominated the variability. AW inflow is partly wind driven, and we found an increased wind-driven AW inflow (Fig. 11 b). This increased OHT would then alone also have contributed to ice loss, especially in the Barents Sea, as outlined by Smedsrud et al., (2013).

Heat anomalies and melting of Greenland glaciers: The warming on the NE Greenland shelf of about +0.5°C since the 1970's (Fig. 10 a) is quite typical for the other Arctic shelf seas. In the Barents Sea the warming has been twice as large (Fig. 9), but similar warming is otherwise simulated for all the Arctic shelf seas (not shown). The warming is also comparable to observations of AW temperature in the Fram Strait (79°N) and in the West Spitsbergen current (76°N) clearly indicating that AW is the advective source (Muilwijk et al., 2018). There is a large re-circulation of AW in the Fram Strait (Hatterman et al., 2016), a water mass termed Return AW, and this has warmed about +1°C since the 1950's (Fig. 5). The simulated warming on the shelf (Fig. 10 a) is similar to that observed at the margins of the largest ice shelf in NE Greenland (Nioghalvfjerdsfjorden; Lindeman et al., 2020; Mouginot et al., 2015). The warming of AW inflow at the GSR is smaller than the warming in Fram Strait (Fig. 5). This suggests that the relatively low Nordic Seas heat loss since 2000 has played a role (Fig. 2), and that part of the warming is caused by a smaller than normal heat loss within the Nordic Seas (Fig. 2). The +0.5°C warming since the 1970's has clearly driven increased melting of marine terminating glaciers, and the inferred retreat of ~0.5 km is substantial and about 50% of that observed (Fig. 10 b), consistent with additional retreat resulting from dynamic thinning of the glaciers in response to the forced retreat. The atmospheric warming, dictated by the 20CR forcing, is a clear manifestation of global warming. It too contributes to driving glacier retreat through the enhanced submarine melting associated with an increasing release of surface melt at depth (Jenkins, 2011; Slater et al., 2016). According to the employed data-constrained parameterization (Slater et al., 2019), the ocean and atmospheric variability contribute in approximately equal parts to the glacier retreat (Fig. 10).

Heat fluxes and CO_2 uptake: The relationship between CO_2 flux and heat transport and loss is a consequence of the increased CO_2 solubility in colder waters, i.e., the larger the heat loss, the larger the CO_2 uptake. Watson et al. (1995) derived an equation for the heat loss driven CO_2 uptake: ($\frac{-Q\ DIC\ \tau}{c_p\ R_f}$), where DIC is Dissolved Inorganic Carbon concentration, τ is the isochemical $p$$CO_2$ temperature dependency (Takahashi et al, 1993), and R_f the Revelle factor. Q and c_p are heat loss and heat capacity as in Eq (1). Using representative numbers for the early 20th century Arctic Ocean ($Q = 160$ TW; Atlantic inflow DIC = 2070 μmol kg^{-1} and $R_f = 11$) we find a heat loss driven CO_2 uptake of 120 Mt C yr^{-1}. This increases to 160 Mt yr^{-1} for a heat loss of 210 TW, which has been the values reached in the last decades (Fig. 2). The magnitude and increase of this heat loss inferred fluxes are somewhat smaller than the ~170 Mt yr^{-1} increasing to ~230 Mt yr^{-1} (Fig. 6). This might be related to the large uncertainties involved in this calculation, it is for example highly sensitive to the exact heat flux value used, and also the complete neglect of biological and anthropogenic fluxes. Naturally also the regressions in Fig. 6 (Table A) have their uncertainties. Nevertheless, the results from the three lines of evidence altogether presented, the solubility considerations (Sec. 2.3), Fig. 6, and the heat loss dependency equation here, give results of the same order of magnitude, showing that the bulk of the CO_2 uptake in the Arctic Ocean is driven by the ocean cooling, and that the increased cooling has caused a larger CO_2 uptake.

One might ask whether the difference between increase in annual CO2 uptake derived from the heat fluxes here (40 Mt yr^{-1}) and that derived from the regressions earlier (60 Mt yr^{-1}) is a consequence of the fact that the increased heat loss has occurred in the Barents and Polar Sea associated with the retreating sea ice. This exposes waters undersaturated with CO_2 to the atmosphere and enables primary production, which lead to a larger CO_2 uptake than anticipated from heat loss increases alone (Anderson & Kaltin, 2001). This might be the reason for why the changes in Polar and Barents seas CO_2 uptake since 1998 relates more strongly to sea-ice cover than heat loss (Fig. 6). Disentangling the impacts of each specific process is best done with a fully coupled model including carbon cycle components. Such studies should also consider the potential impacts of variations in the horizontal ocean carbon transports on the air-sea carbon flux in the Arctic Ocean; as these fluxes are much larger than the air-sea flux (Jeansson et al., 2011). More explicit accounting of changes in natural vs. anthropogenic carbon fluxes would also be worthwhile.

Heat anomalies and production of Overflow Water (OW): NorESM simulates mean properties and long-term trends of the dense waters flowing southward across the GSR reasonably well (Fig. 5). Since the mid-1990s the observed OW transport has remained steady, but the temperature has increased (Hansen et al., 2016; Jochumsen et al., 2017; Mastropole et al., 2017; Østerhus et al., 2019), this is well captured by the NorESM (Fig. 8). Between 1998 and 2002 the observed AW inflow temperature and volume transport increased, resulting in a 7% increase in OHT (Tsubouchi et al., 2020), qualitatively similar, but not identical to the NorESM simulations (Fig. 4). The recent interior warming in the Iceland and Greenland Seas after 2000 (Fig. Q) is also partly captured by NorESM (Fig. 5). The density of the intermediate waters have been stable over the same time period due to a compensating increase in salinity (Fig. Q; Lauvset et al., 2018). This balance may imminently change as a result of the pronounced freshening of the inflowing AW (Mork et al., 2019), especially if the heat loss continues to decrease as could be expected in a warming climate (Moore et al., 2015). On the other hand may the sea ice retreat lead to more favorable conditions for dense water formation at new locations (Lique & Thomas, 2018), as recently observed in the Barents Sea (Skagseth et al., 2020), along the East Greenland Current (Våge et al., 2018), and north of Svalbard (Pérez-Hernández et al., 2019; Athanase et al., 2020).

6 Conclusion

Global Warming and Arctic sea ice loss have been ongoing and well documented for at least 30 years. The Arctic sea ice loss is consistent with a larger loss of heat from the ocean to the atmosphere, mostly occurring in the Barents and Polar Seas. This increased heat loss from the inflowing Atlantic Water (AW) is in itself connected to a larger inflow of AW. But there has additionally been an increased wind forcing of the AW inflow in the Nordic Seas, and the two together explain the long-term AW increase of about +1 Sv over the last century. This increased AW volume inflow is the main explanation for the increased heat transport to the Arctic Ocean from about 150 TW in 1900 to 200 TW today. The partitioning between overturning (dense water and Overflow Water (OW) formation) and the horizontal boundary current (Polar Water (PW) formation) has remained roughly equal over the last century, but temperature variability plays a larger role in the overturning part.

The gradual cooling of the AW as it circulates the Arctic Ocean from its entry across the Greenland-Scotland Ridge (GSR) mostly occurs in the Nordic Seas. The year-to-year variability of this (winter) cooling is dictated by the atmospheric forcing manifested in the variability of occurrence of low pressure systems over Scandinavia, which drive Cold Air Outbreaks (CAOs) with strong winds off the sea ice in the Polar Sea. The AW cooling in the Nordic Seas explains about 50% of the CO2 uptake of the entire Arctic Ocean, but the contribution from the Barents and Polar Seas are increasing with the diminishing sea ice cover.

The sea ice cover of the Arctic Seas is set to further decrease in the future. This will contribute to more open water and a larger ocean heat loss. Such an increased heat loss – unless compensated elsewhere – will again require a larger (baroclinic) inflow of AW, and a larger Ocean Heat Transport (OHT). This heat transport takes place mostly in the horizontal inflow of AW on the eastern side of the GSR, and there has been a consistent increase in this boundary flow of about + 1 Sv over the last century, which is thus expected to continue to increase. Consistently we expect that the main processes illustrated in Fig. 12 are all set to increase; warming on the Arctic shelves, the ocean contribution to melting of glaciers on Greenland, and the future Arctic Ocean CO2 uptake.

The future production of dense water is more uncertain, as it is wedged between the increased larger heat transported in, and the larger heat loss at the surface. There is in addition the natural climate variability exemplified here by the wind forcing of the AW and the CAOs. These fluctuations remain hard to dissect – not to say predict, and a century of variability may not be long enough to properly disentangle the governing mechanisms.

Acknowledgments

This work was supported by the Bjerknes Center for Climate Research, and furthermore the Norwegian Research Council through the Nansen Legacy Project (Grant#276730) and the U.S. Norway Fulbright Foundation. L. H. Smedsrud particularly thanks the Foundation for the Norwegian Arctic Chair grant 2019-20 that made much of this work possible.

We acknowledge the World Climate Research Programme, which, through its Working Group on Coupled Modelling, coordinated and promoted CMIP6. We thank the NorESM Consortium for producing and making available their simulations, the ESGF for archiving and providing access, and the multiple funding agencies who support CMIP6 and ESGF. We would also like to thank all those who collected valuable observations over the last century that made this study possible.

Data Availability Statement

Monthly fields from the NorESM2-LM for the period 1958-2018 (Bentsen et al., 2019) have been provided through the Ocean Model Intercomparison Project Phase 2 (OMIP2) experiment as part of the Coupled Model Intercomparison Project Phase 6 (CMIP6, Eyring et al., 2016), and are available for download on the Earth System Grid Federation (ESGF) website: https://esgf-node.llnl.gov/search/cmip6/. Monthly fields of NorESM for the time period 1900-2009 are available upon request. 20CRv2c Reanalysis data are freely available for download at https://portal.nersc.gov/project/20C_Reanalysis/. Kola section data is from the Knipovich Polar Research Institute of Marine Fisheries and Oceanography available through ICES (International Council for Exploration of the Seas; https://ocean.ices.dk/core/iroc)

Abbreviations

20CRv2 - 20th Century atmospheric Reanalysis forcing, AMO - Atlantic Multidecadal Oscillation, AW - Atlantic Water, CAO – Cold Air Outbreaks, GSR - Greenland-Scotland Ridge, NAO - North Atlantic Oscillation, NorESM - Norwegian Earth System Model, OHT - Ocean Heat Transport, OW - Overflow Water, PW - Polar Water, RAW - Return Atlantic Water, SIC - Sea Ice Concentration, SSS - Sea Surface Salinity, SST - Sea Surface Temperature.

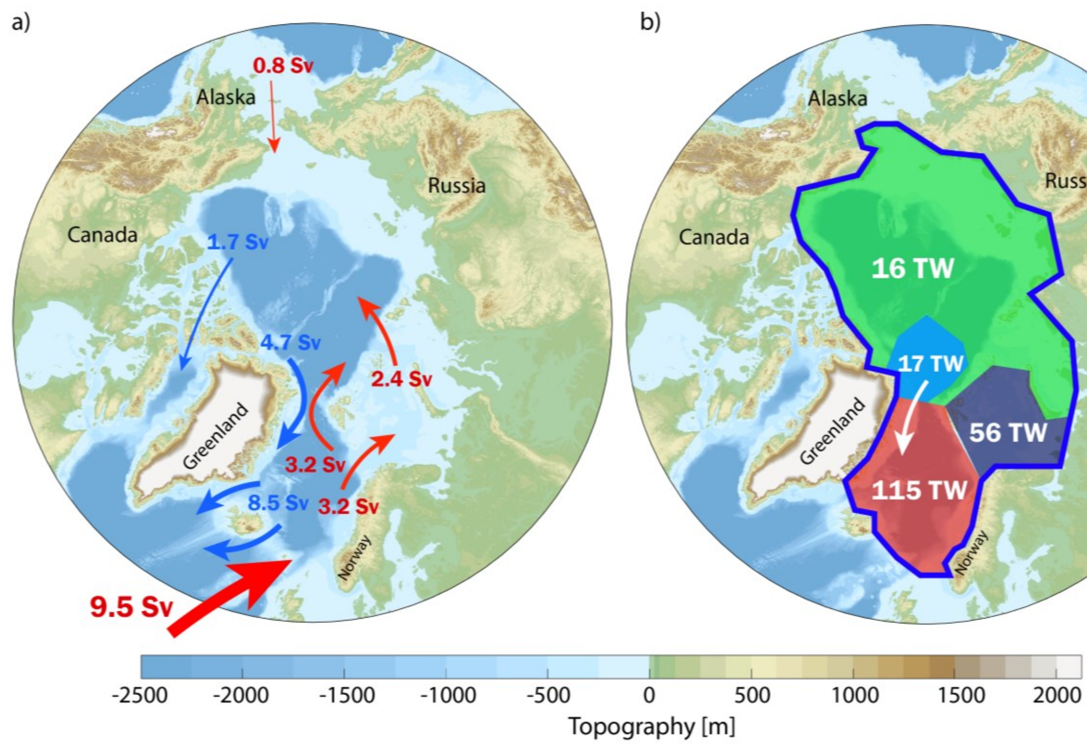

Figure 1: The mean simulated Arctic Ocean volume transport and heat loss. a) The northward (red arrows) and southward flows (blue arrows) are scaled so that the width represents volume transports in Sv. b) The heat loss in the Nordic Seas (red, area of 2.5 mill km²), the Barents Sea (black, 1.5 mill km²) and the Polar Sea (Green, 8.4 mill km²) in Tera Watts (1 TW = 1×10^{12} W). The cyan region represents the annual mean sea ice area export (~1 mill km²) from the Polar Sea to the Nordic Seas (white arrow). This heat is released to the Polar Sea atmosphere when the sea ice forms, with subsequent loss of heat from the Nordic Seas when the sea ice melts, contributing to the 115 TW cooling indicated in the figure.

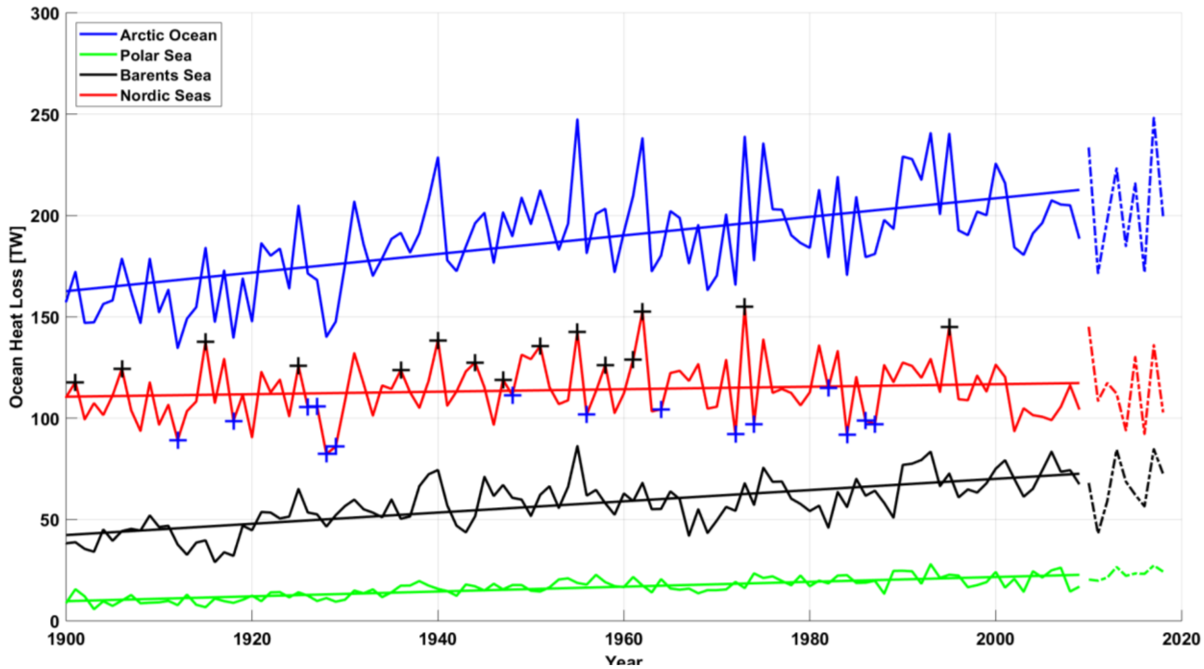

Figure 2: The simulated annual heat loss of the Arctic Seas in NorESM.

The simulated, annual mean ocean heat loss (TW) from the 20CR (1900-2009; solid lines) and the JRA forced (2010-2018; dashed lines) runs, with colors from Fig. 1b. The mean cooling of the Arctic Ocean is 187 TW (Table 1). For the Nordic Seas the 15 years of highest (black crosses) and lowest (blue crosses) annual de-trended heat losses are indicated.

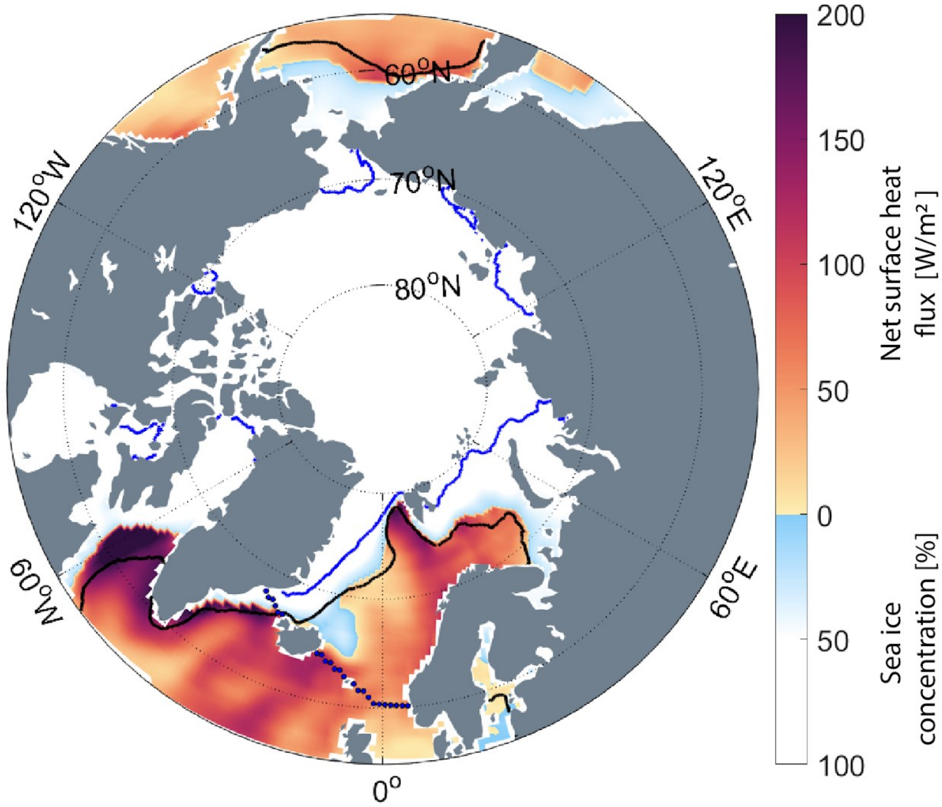

Figure 3: The simulated annual mean surface heat flux (W/m^2, warm colors) and Sea Ice Concentration (SIC, percentage, cold colors) between 1900-2000.

The centennial mean observed sea ice extent for September (blue line) and March (black line) has been added from Walsh et al. (2017). The dotted blue line shows the location of the Greenland-Scotland Ridge (GSR) as used here and extended directly east along 60 °N from Shetland to Bergen.

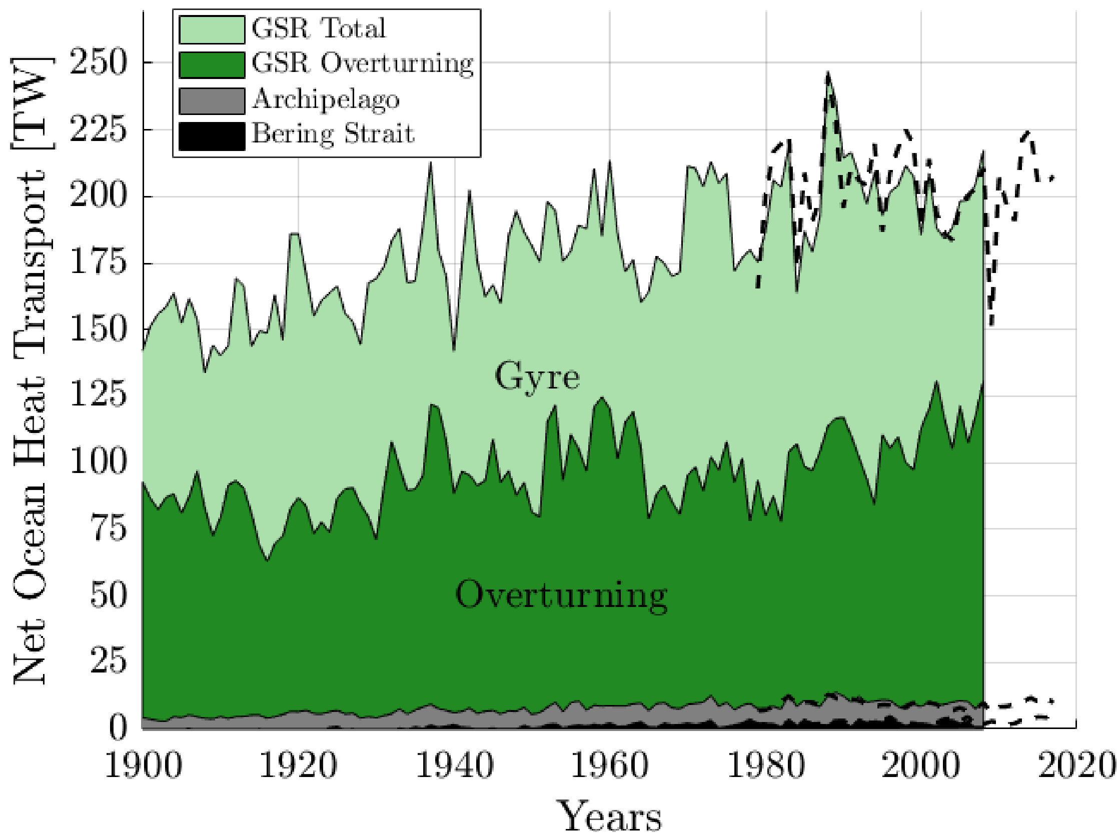

Figure 4: The simulated, annual mean Arctic ocean heat transport.

The contributions from the individual straits are calculated using 0 °C as reference, and show the Bering Strait inflow, the outflow through the Canadian Archipelago, and the inflow and outflow across the Greenland-Scotland Ridge (GSR). The centennial mean Arctic Ocean heat transport is 179 TW. The top line shows the Arctic Ocean total independent of a reference temperature. The dashed line is the total NorESM JRA forced version updated to 2018. The heat transport across the GSR has been decomposed into a horizontal gyre and a vertical overturning contribution.

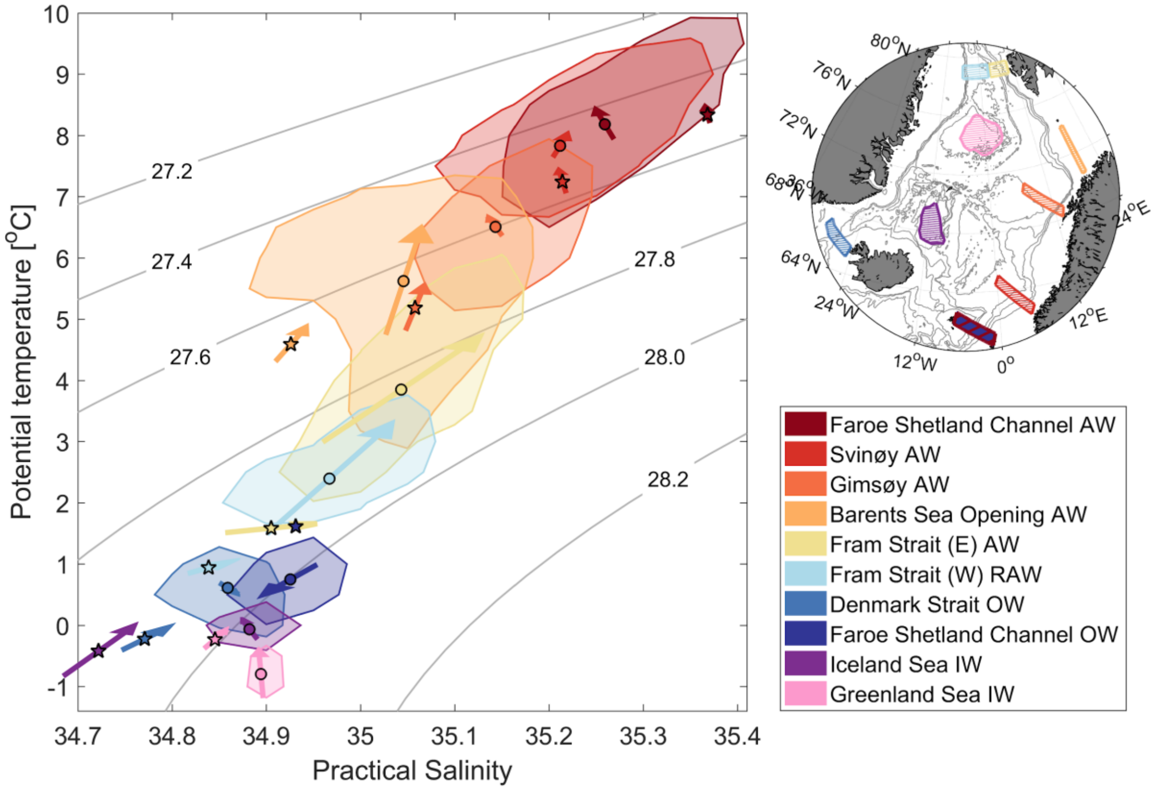

Figure 5: Observed and simulated Nordic Seas thermohaline water mass properties (1950-2019). Geographical regions, with color coding, are marked on the map. The TS-range of each water mass is based on the frequency of occurrence and indicated by the colored patches outlining 60 percent of the observations. Color-filled dots show observed median values, and related arrows show the linear trends. Similarly, colored stars show simulated NorESM median values and the related arrows the linear trends (1950-2009). Vertical constraints for defining the water masses are as follow: Atlantic Water (AW) and Returning Atlantic Water (RAW) by the depth of maximum temperature below 100 m (± 50 m); Overflow Water (OW) by density above 27.8 kg/m³ and above the sill depths (650 m for the Denmark Strait and 840 m for the Faroe Shetland Channel); Intermediate Water (IW) by the typical mixed-layer depths 150-350 m in the Iceland Sea and 500-1500 m in the Greenland Sea. Observations from Brakstad et al. (In Prep).

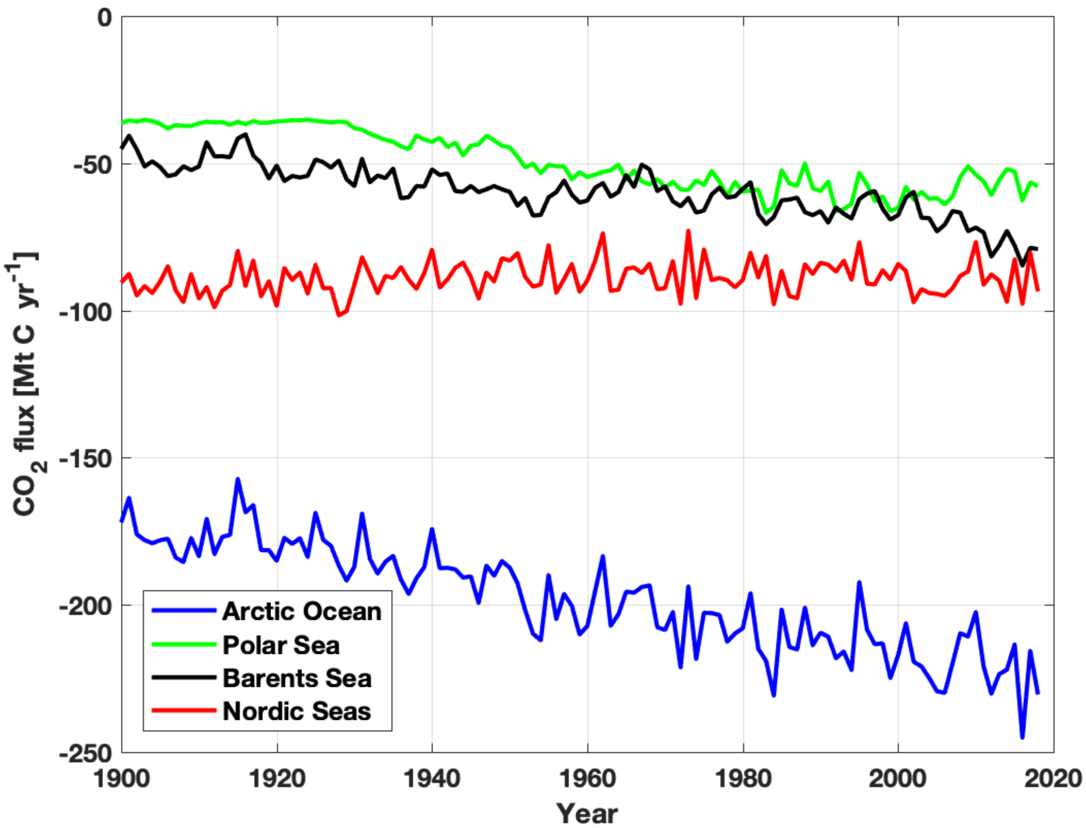

Figure 6: CO_2 uptake (Mt C/yr) as a function of simulated (NorESM) surface forcing.

For the Barents and Polar Seas the most important parameter is the sea ice cover, whereas in the Nordic Seas heat loss is best at explaining observed variability. The negative values show ocean uptake of CO_2. Areas used to convert fluxes into Mt C are from Table 1.

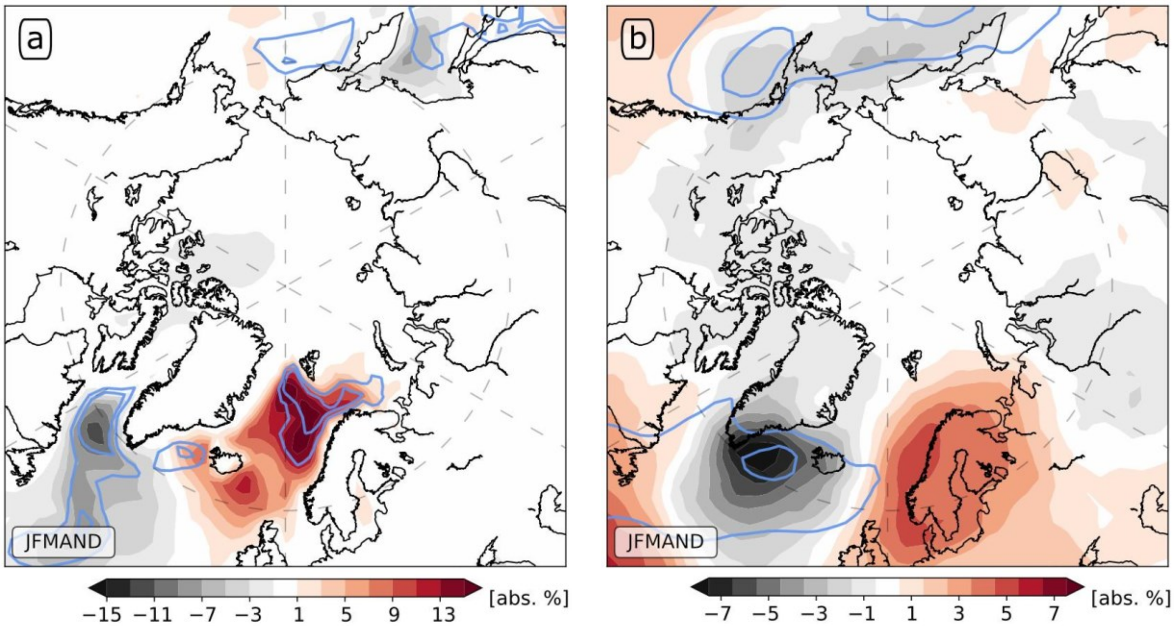

Figure 7: Anomalous frequency of occurrence (%) of (a) cold air outbreaks (CAOs) and (b) extratropical cyclones.

Plots show the 15 years with the largest versus smallest Nordic Seas heat loss based on the detrended centennial time series (black and blue symbols in Fig. 2). Contour lines show the respective climatology with contours at 20 and 30 absolute % frequency of occurrence. The anomalies are based on 20CRv2c and for the extended winter season within the same calendar year (January through April, and then November and December).

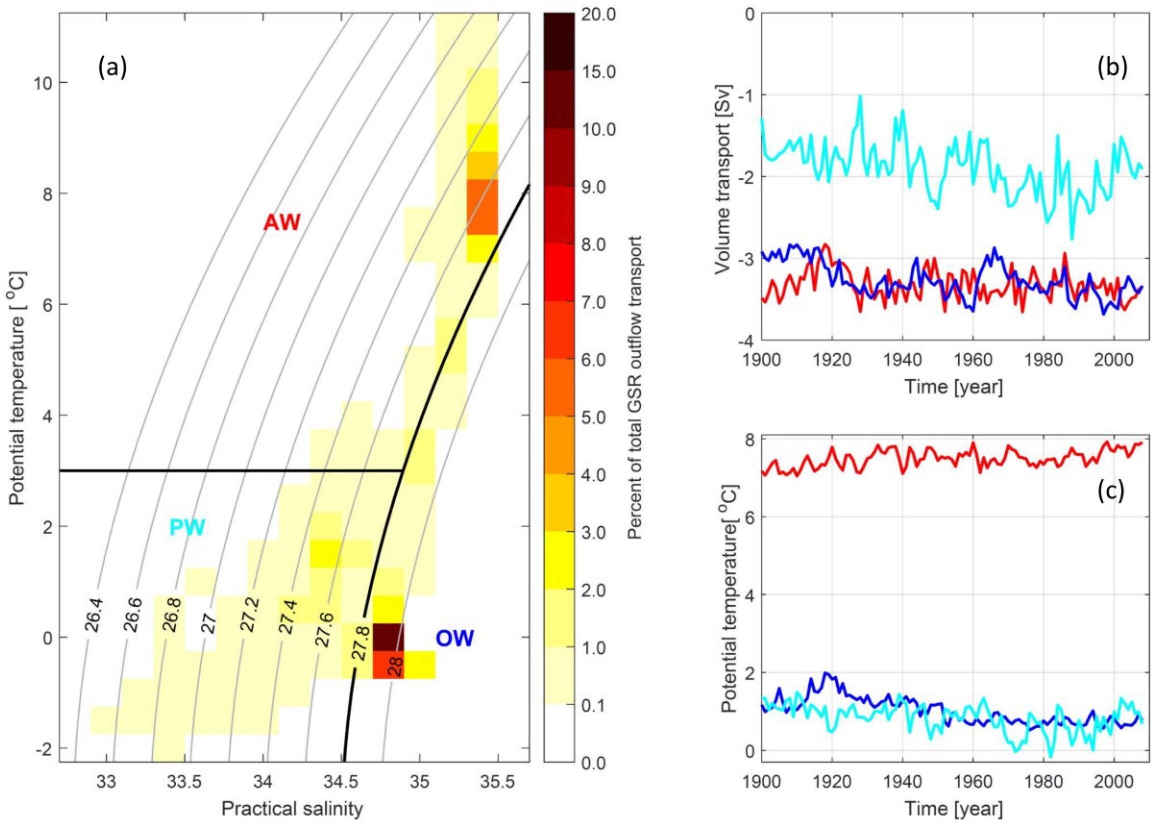

Figure 8: Simulated properties of the Greenland-Scotland ridge (GSR) outflow.

a) shows the contribution (%) to GSR outflow as a function of temperature and salinity. The outflow is divided into three main water masses: Overflow Water (OW), Polar Water (PW) and outflowing Atlantic Water (AW), b) shows annual mean volume transport (Sv) and c) potential temperature (°C) for each water mass, with color coding as in Fig. 2.

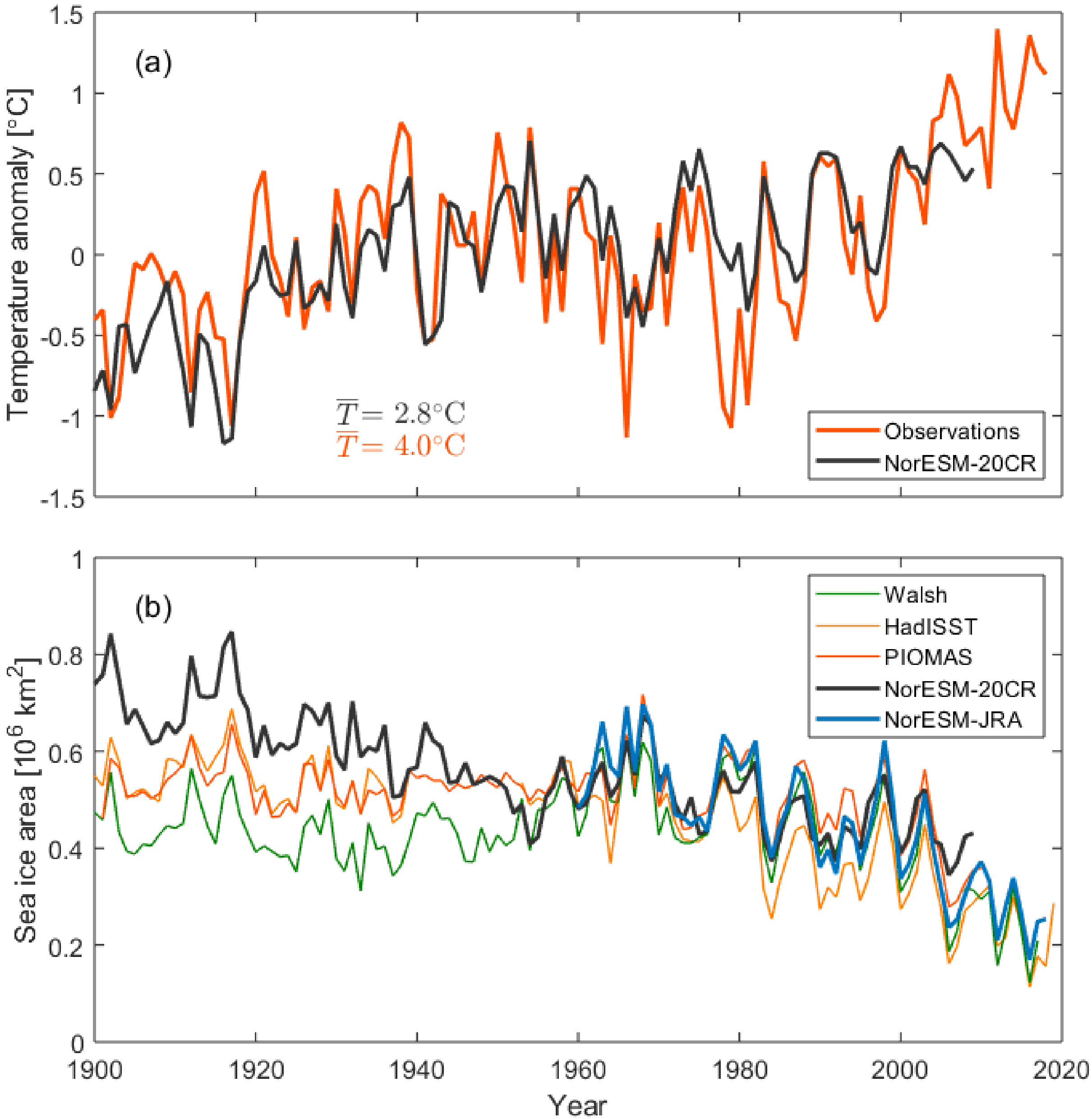

Figure 9: Simulated and observed Barents Sea temperature and sea ice variability since 1900. (a) Observed (orange; ICES 2020) and simulated (black) annual mean temperature anomalies (°C) relative to the 1900-2009 mean temperature of respectively 4.0 °C and 2,8 °C along the Kola Section. (b) Annual mean sea ice area (10^6 km^2) in the Barents Sea from NorESM and reconstructions based on observations or simulations (HadISST; Rayner et al. 2003, Walsh et al. 2017, and PIOMAS-20C; Schweiger et al. 2019).

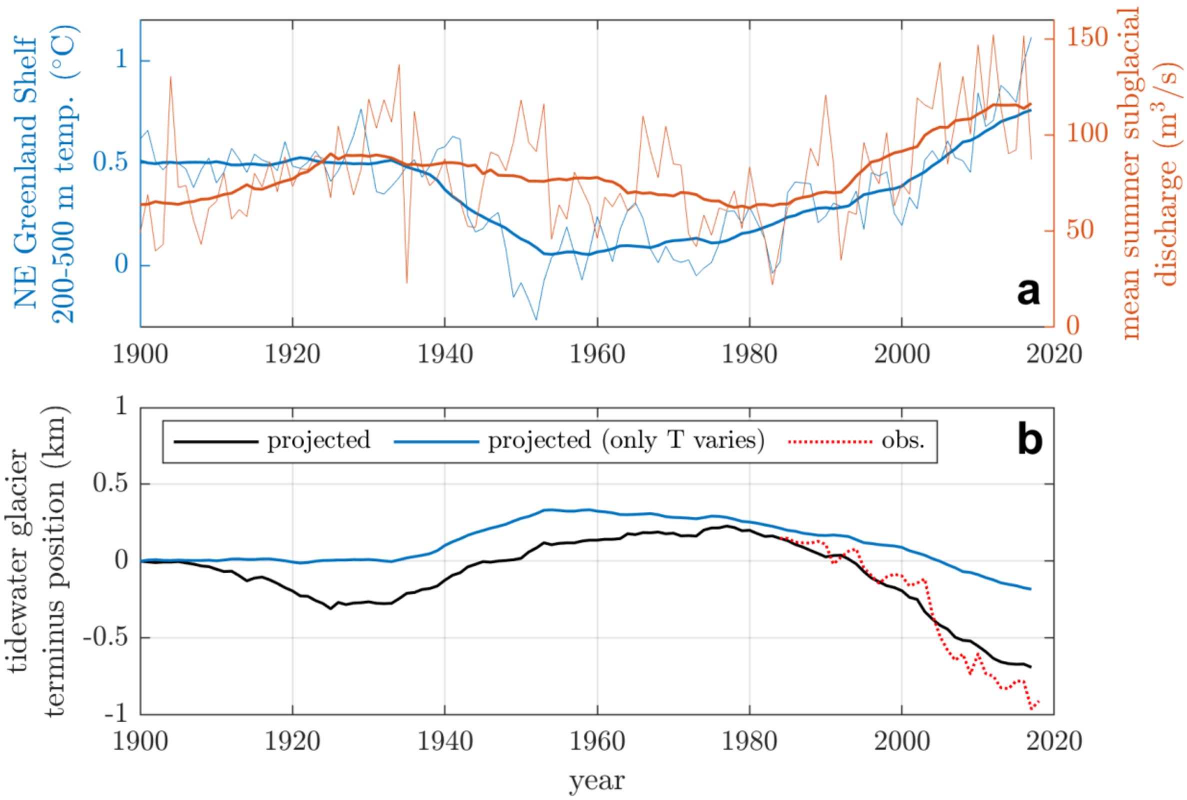

Figure 10: Impact of ocean changes on the NE Greenland ice sheet.

(a) NorESM-simulated ocean temperature averaged over the NE Greenland continental shelf between the depths of 200 and 500 m (°C, blue, left axis) and simulated summer liquid freshwater flux (subglacial discharge) from NE Greenland's marine-terminating glaciers (m^3/s, red, right axis; Fettweis et al., 2017). (b) Simulated advance or retreat of NE Greenland's marine-terminating glaciers. The projected terminus position (km, black) is based on the parameterisation described by Slater et al. (2019), using the NorESM ocean temperature and subglacial discharge shown in (a) as inputs. The blue line shows the projected terminus position when subglacial discharge is held constant at its mean 1900-2017 value, and thus isolates the impact of the ocean on the glaciers. The red dashed line shows the observed terminus positions since 1984 (Slater et al. 2019). All values are averaged over all glaciers in the region and more negative position values indicate a more retreated glacier.

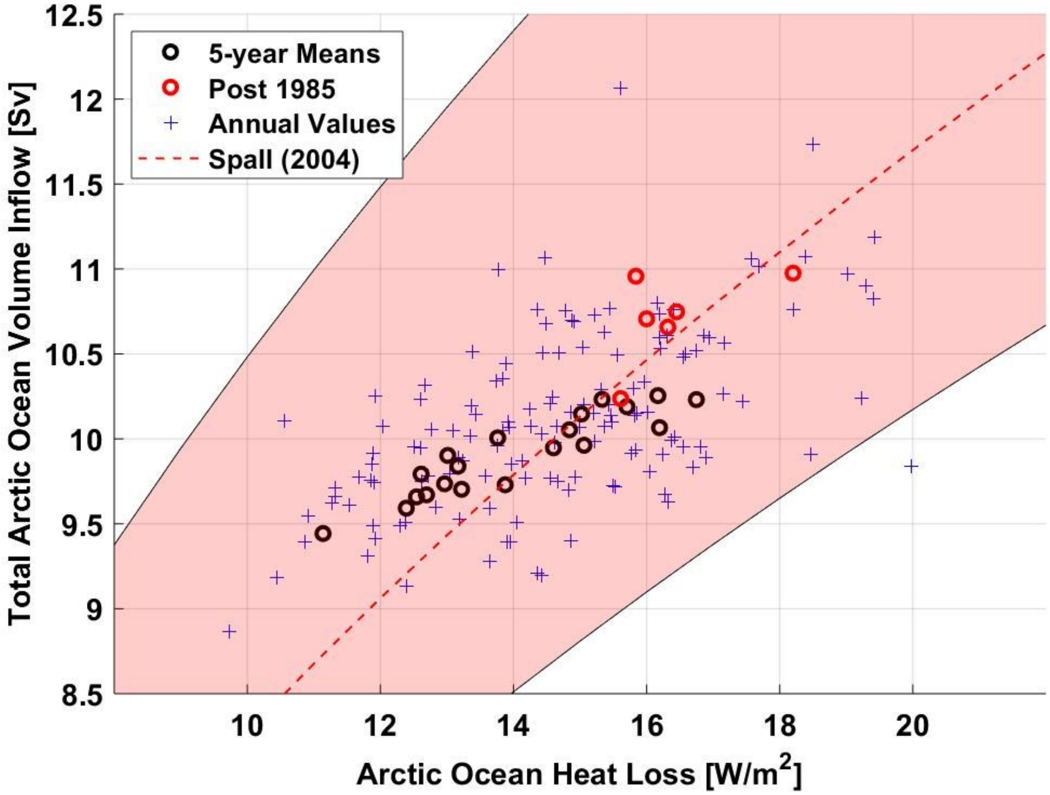

Figure 11 a): Inflow towards the Arctic Ocean as a function of heat loss.

Simulated (NorESM) annual values and the 5-year means of the inflow (Sv) towards the Arctic Ocean across the Greenland Scotland Ridge and the Bering Strait. The dashed line is from Spall (2004), analytically derived from the heat loss (abscissa) and representative values of the basin radius, Coriolis parameter, the slope width, and the 500 m inflow depth of the GSR. The red envelope spans out inflow values based on varying these parameters as explained in the text.

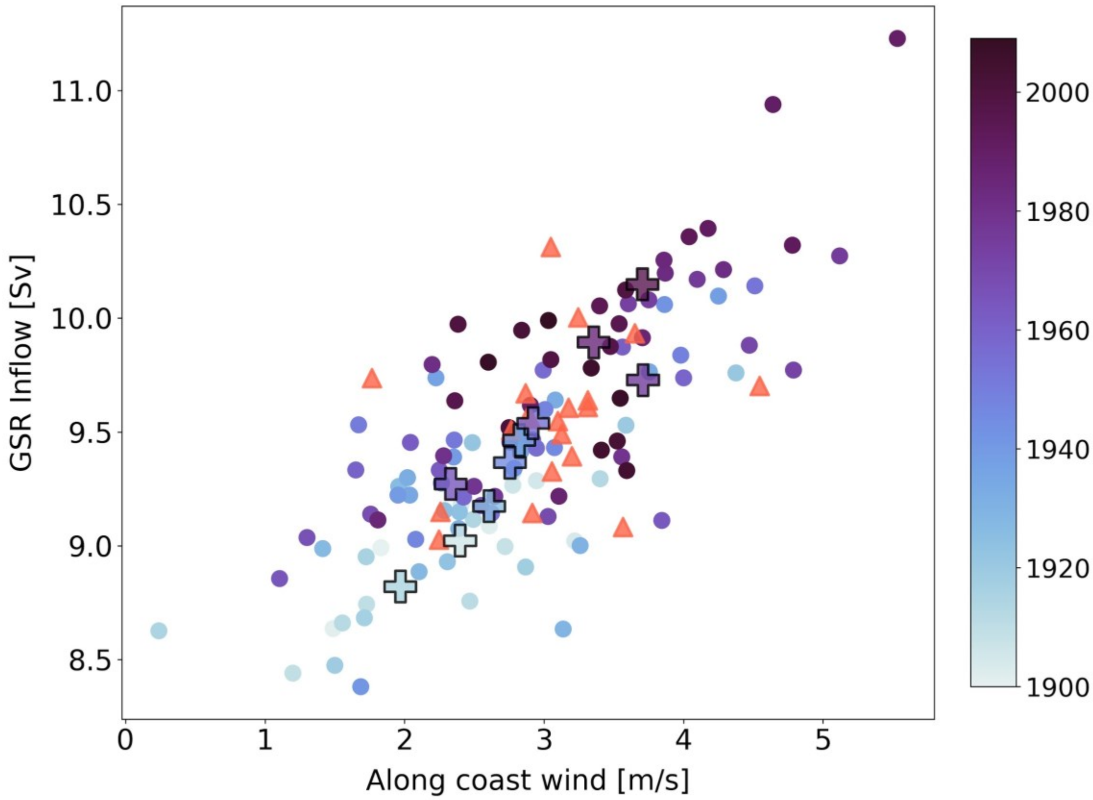

Figure 11 b): Inflow and wind forcing.

Circles show the simulated annual (spatial) mean values of along-coast wind speed (m/s) between the Faroes-Shetland and the Svinøy sections off the Norwegian west coast, and the overall poleward flow (Sv) across the GSR. The correlation coefficient is *r*=0.78. Larger crosses show decadal means. Color coding represent the simulation year. Observed volume transport from the eastern Svinøy branch (NMDC 2020, 1996-2016) and observed (bias-corrected) wind speed from Utsira (NCSC 2020) are included as orange triangles, using a constant addition of +5.14 Sv representing the outer branch (value of +4.14 Sv) and inflow west of Iceland (+1 Sv).

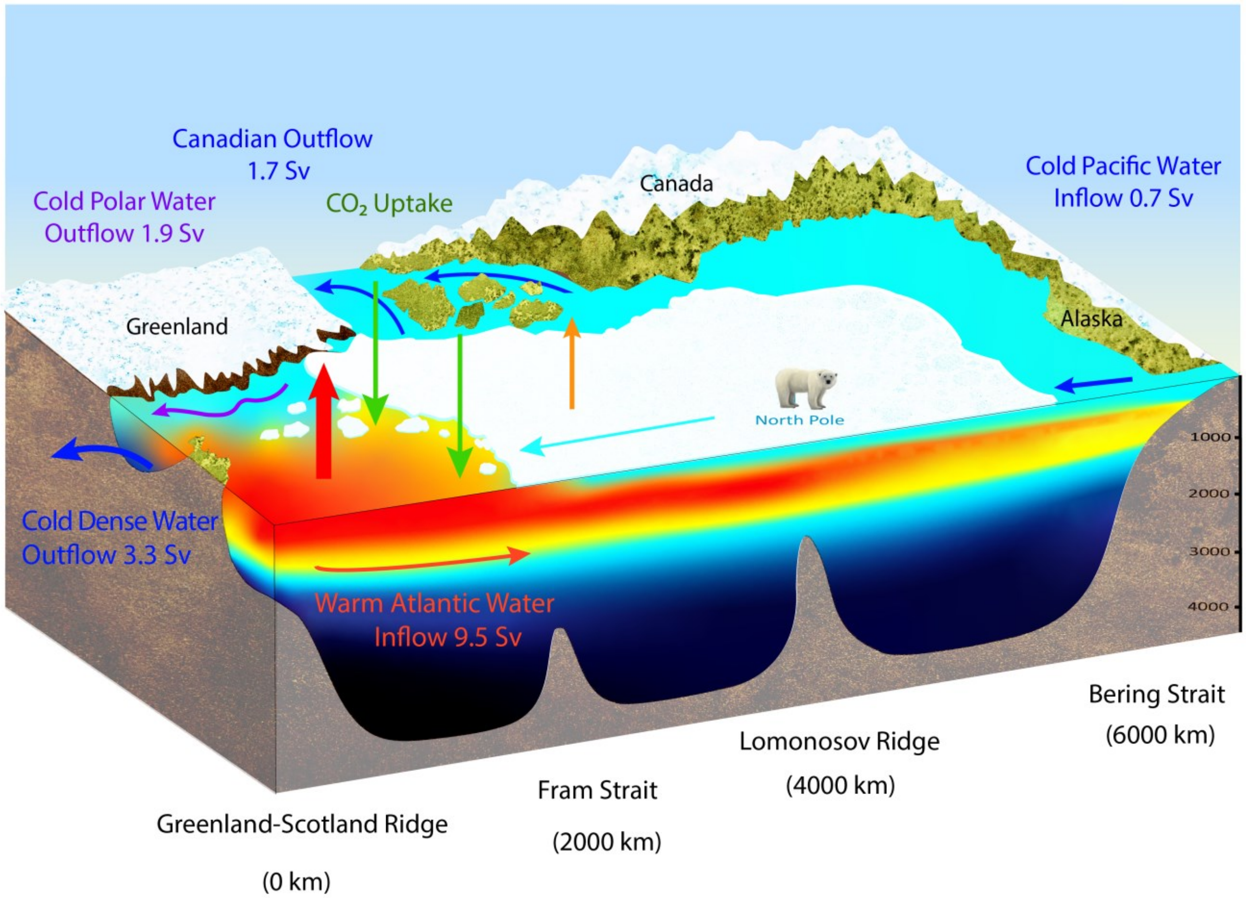

Figure 12: The summary sketch, how it all works.

The warm AW inflow and its contributions to the 1) Nordic Seas heat content, 2) deep and dense OW properties, 3) CO_2 uptake, 4) Greenland melting, and 5) Arctic sea ice cover. The vertical red arrow illustrates the large cooling in the Nordic Seas, and the orange arrow the smaller cooling in the Polar Sea. The eastern half of the Nordic Seas and the Arctic Ocean is not shown, but the area and bathymetry is correctly scaled. The cyan arrow represents the systematic sea ice drift towards the Fram Strait.

Figure made by: Marlo Garnsworthy - Wordy Bird Studio – but it is purpose made for this paper.

List of Figures

Table 1. Simulated centennial annual mean properties for the Arctic Seas from the NorESM for 1900-2009. The heat loss is the heat flux multiplied by the area of each sea. The CO_2 uptake is estimated as described in the methods based on heat flux and Sea Ice Concentration (SIC). All values, including Sea Surface Temperature (SST) and Sea Surface Salinity (SSS) are averages over the seas shown in Fig. 1. Heat loss trends that are significant at the 95% level is indicated by a (*) $p < 0.05$. TW (Tera Watt = 10^{12} W).

	Area	Heat Loss	Heat Flux	SIC	SST	SSS	CO_2 Uptake	Heat Loss Trend/Century
Unit	[10^6 km²]	[TW]	[W/m²]	[%]	[°C]	[g/kg]	Mt C/yr	TW/100 yr
Polar Sea	**8.36**	**15.89**	**1.90**	**94.8**	**-1.6**	**31.3**	**55.7**	**11.9***
Barents Sea	**1.47**	**56.54**	**38.10**	**52.8**	**0.9**	**34.2**	**66.7**	**27.7***
Nordic Seas	**2.54**	**114.75**	**45.08**	**28.0**	**3.0**	**34.5**	**88.3**	**6.2**
Arctic Ocean	**12.38**	**186.80**	**15.08**	**75.7**	**-0.3**	**32.3**	**209.9**	**45.8***

Table 2. Mean ocean transports in relevant Arctic Seas sections (1900-2000). Positive volume transport values are northward. The Ocean Heat Transport (OHT) is relative to 0 °C for all sections. A positive OHT with a negative (southward) volume transport implies that the temperature is lower than 0 °C. Numbers are rounded to the closest 0.1 Sv.

	Volume	OHT
Unit	[Sv]	[TW]
Bering Strait net	**+0.7**	**+0.9**
Canadian Archipelago net	**-1.7**	**+6.6**
GSR net transport	**+1.0**	**+172**
Arctic Ocean net	**0.0**	**+179**
GSR AW Inflow	**+9.5**	**+285**
GSR total outflow	**-8.5**	**-113**
GSR OW	**-3.3**	**-9**
GSR PW	**-1.9**	**-3**
GSR AW outflow	**-3.3**	**-101**
Fram Strait net transport	**-1.5**	**+15**
Fram Strait Northwards	**+3.2**	**+5**
Fram Strait Southwards	**-4.7**	**+10**
Barents Sea Opening net	**+2.4**	**+47**
Barents Sea Opening Northward	**+3.2**	**+53**
Barents Sea Opening Southward	**-0.8**	**-6**

References

Aagaard, K., Swift, J. H., & Carmack, E. C. (1985), Thermohaline circulation in the Arctic Mediterranean Seas, *J. Geophys. Res.*, 90 (C3), 4833– 4846, doi:10.1029/JC090iC03p04833.

Anderson, L. G. & Kaltin, S. (2001) Carbon fluxes in the Arctic Ocean - potential impact by climate change, Polar Res, 20, 225-232, doi:10.3402/polar.v20i2.6521

Anderson, L. G., Jutterstrom, S., Hjalmarsson, S., Wahlstrom, I., & Semiletov, I. P. (2009) Out-gassing of CO2 from Siberian Shelf seas by terrestrial organic matter decomposition, Geophys Res Lett, 36, doi:10.1029/2009GL040046

Arrigo, K. R., & G. L. van Dijken (2015), Continued increases in Arctic Ocean primary production, Progress in Oceanography, 136, 60-70, doi:10.1016/j.pocean.2015.05.002.

Asbjørnsen, H., Årthun, M., Skagseth, Ø., & Eldevik, T. (2019). Mechanisms of ocean heat anomalies in the Norwegian Sea. J. Geophys. Res. Oceans, 124, 2908–2923. doi:10.1029/2018JC014649

Asbjørnsen H., Årthun, M., Skagseth, Ø., & Eldevik, T. (2020). Mechanisms underlying recent Arctic Atlantification. Geophysical Research Letters, 47, e2020GL088036. doi:10.1029/2020GL088036

Athanase et al. (2020) Atlantic Water Modification North of Svalbard in the Mercator Physical System From 2007 to 2020. Journal of Geophysical Research: Oceans, 125, 10, doi:10.1029/2020JC016463

Barnston, A. G., & Livezey, R. E. (1987) Classification, seasonality and persistence of low-frequency atmospheric circulation patterns. Mon. Wea. Rev., 115:1083–1126, doi:10.1175/1520-0493(1987)115<1083:CSAPOL>2.0.CO;2

Bamber, J., van den Broeke, M., Ettema, J., Lenaerts, J., & Rignot, E. (2012) Recent large increases in freshwater fluxes from Greenland into the North Atlantic. Geophysical Research Letters, 39, L19501. doi:10.1029/2012GL052552

Bamber, J. L., Tedstone, A. J., King, M. D., Howat, I. M., Enderlin, E. M., van den Broeke, M. R., & Noel, B. (2018). Land ice freshwater budget of the Arctic and North Atlantic Oceans: 1. Data, methods, and results. Journal of Geophysical Research: Oceans, 123, 1827–1837, doi:10.1002/2017JC013605

Behrendt, A., Sumata, H., Rabe, B., & Schauer, U. (2018). UDASH – Unified Database for Arctic and Subarctic Hydrography, Earth Syst. Sci. Data, 10, 1119–1138, doi:10.5194/essd-10-1119-2018.

Bentsen, M. et al. (2013). The Norwegian Earth System Model, NorESM1-M - Part 1: Description and basic evaluation. Geoscientific Model Development Discussions, 5, 2843–2931. doi:10.5194/gmdd-5-2843-2012

Bentsen, M. et al. (2019) NCC NorESM2-LM model output prepared for CMIP6 OMIP omip2. Version 20200401. Earth System Grid Federation. doi:10.22033/ESGF/CMIP6.8089

Berx, B., B. Hansen, S. Østerhus, K. M. Larsen, T. Sherwin, & K. Jochumsen (2013) Combining in situ measurements and altimetry to estimate volume, heat and salt transport variability through the Faroe–Shetland Channel, Ocean Sci., 9, 639–654, doi:10.5194/os-9-639-2013

Bjerknes, J. (1964) Atlantic Air-Sea Interaction, Editor(s): H.E. Landsberg, J. Van Mieghem, Advances in Geophysics, Elsevier,10, 1-82, doi:10.1016/S0065-2687(08)60005-9.

Bjørk, A., Kjær, K., Korsgaard, N. et al. (2012) An aerial view of 80 years of climate-related glacier fluctuations in southeast Greenland. Nature Geosci 5, 427–432, doi:10.1038/ngeo1481

Bleck, R., Rooth, C., Hu, D., & Smith, L. T. (1992) Salinity-driven Thermocline Transients in a Wind- and Thermohaline-forced Isopycnic Coordinate Model of the North Atlantic. J. Phys. Oceanogr., 22, 1486–1505, doi:10.1175/1520-0485(1992)0222.0.CO;2

Böning C.W., & Bryan, F.O. (1996). Large-scale transport processes in high-resolution circulation models. in The Warmwatersphere of the North Atlantic Ocean, W. Krauss, Ed., Gebrüder Borntraeger, 91–128.

Brennan, M. K., Hakim, G. J., & Blanchard-Wrigglesworth, E. (2020). Arctic sea-ice variability during the instrumental era. Geophys. Res. Lett. 47, e2019GL086843. doi:10.1029/2019GL086843

Bringedal, C., Eldevik, T., Skagseth, Ø., Spall, M., Østerhus, S. (2018). Structure and forcing of observed exchanges across the Greenland-Scotland Ridge. Journal of Climate, 31, 9881–9901, doi:10.1175/JCLI-D-17-0889.1

Bueh, C., & Nakamura, H. (2007). Scandinavian pattern and its climatic impact. Quarterly Journal of the Royal Meteorological Society: A journal of the atmospheric sciences, applied meteorology and physical oceanography, 133(629), 2117-2131, doi:10.1002/qj.173

Brakstad, A., Våge, K., Håvik, L., & Moore, G.W.K. (2019): Water Mass Transformation in the Greenland Sea during the Period 1986–2016. JPO, 49 (1), 121–140. doi:10.1175/JPO-D-17-0273.1

Cai, W.-J., et al. (2010), Decrease in the CO2 Uptake Capacity in an Ice-Free Arctic Ocean Basin, Science, 329(5991), 556-559, doi:10.1126/science.1189338.

Carmack, E., Yamamoto-Kawai, M., Haine, T, Bacon, S. (2016). Freshwater and its role in the Arctic Marine System: Sources, disposition, storage, export, and physical and biogeochemical consequences in the Arctic and global oceans. Journal of Geophysical Research Biogeoscience, 121, 675–717, doi:10.1002/2015JG003140

Cassou, C., Terray, L., Hurrell, J. W., & Deser, C. (2004). North Atlantic winter climate regimes: Spatial asymmetry, stationarity with time, and oceanic forcing. Journal of Climate, 17(5), 1055-1068, doi:10.1175/1520-0442(2004)017

Chafik, L. & Rossby, T. (2019). Volume, heat, and freshwater divergences in the subpolar North Atlantic suggest the Nordic Seas as key to the state of the meridional overturning circulation. Geophys Res Lett, 46, 4799–4808, doi:10.1029/2019GL082110

Chafik, L., Hátún, H., Kjellsson, J. et al. (2020) Discovery of an unrecognized pathway carrying overflow waters toward the Faroe Bank Channel. Nat Communications, 11, 3721, doi:10.1038/s41467-020-17426-8

Compo, G.P., Whitaker, J.S., Sardeshmukh, P.D., Matsui, N., Allan, R.J., Yin, X., Gleason, B.E., Vose, R.S., Rutledge, G., Bessemoulin, P., Brönnimann, S., Brunet, M., Crouthamel, R.I., Grant, A.N., Groisman, P.Y., Jones, P.D., Kruk, M.C., Kruger, A.C., Marshall, G.J., Maugeri, M., Mok, H.Y., Nordli, Ø., Ross, T.F., Trigo, R.M., Wang, X.L., Woodruff, S.D. and Worley, S.J. (2011), The Twentieth Century Reanalysis Project. Q.J.R. Meteorol. Soc., 137: 1-28. doi:10.1002/qj.776

Condron, A., & Renfrew, I. A. (2013). The impact of polar mesoscale storms on northeast Atlantic Ocean circulation. Nature Geoscience, 6(1), 34-37, doi:10.1038/ngeo1661

Dickson R. R. et al. (2000). The Arctic Ocean Response to the North Atlantic Oscillation. J. Clim, 13. 2671 – 2696, doi:10.1175/1520-0442(2000)013<2671:TAORTT>2.0.CO;2

Docquier D., Fuentes-Franco R., Koenigk T. & Fichefet T. (2020) Sea Ice-Ocean Interactions in the Barents Sea Modeled at Different Resolutions, Frontiers in Earth Science, 8, doi:10.3389/feart.2020.00172.

Eldevik, T., Nilsen, J.E.Ø., Iovino, D., Olsson, K.A., Sandø, A.B., Drange,H. (2009) Observed sources and variability of Nordic seas overflow. Nature Geoscience 2, 405-409. doi:10.1038/ngeo518.

Eldevik, T. & Nilsen, J. E. Ø. (2013). The Arctic–Atlantic thermohaline circulation. Journal of Climate, 26, 8698–8705, doi:10.1175/JCLI-D-13-00305.1

Fan, S. M., Harris, L. M., & Horowitz, L. W. (2015). Atmospheric energy transport to the Arctic 1979–2012. Tellus A: Dynamic Meteorology and Oceanography, 67(1), 25482, doi:10.3402/tellusa.v67.25482

Fletcher, J., Mason, S., & Jakob, C. (2016). The climatology, meteorology, and boundary layer structure of marine cold air outbreaks in both hemispheres. Journal of Climate, 29(6), 1999-2014, doi:10.1175/JCLI-D-15-0268.1

Friedlingstein, P. et al. (2019) Global Carbon Budget 2019, Earth Syst. Sci. Data, 11, 1783–1838, doi:10.5194/essd-11-1783-2019.

Gebbie, G., & P. Huybers (2011) How is the ocean filled? Geophys Res Lett, 38, L06604, doi:10.1029/2011GL046769

Gillard, L. C., X. Hu, P. G. Myers, & J. L. Bamber (2016) Meltwater pathways from marine terminating glaciers of the Greenland ice sheet, Geophys. Res. Lett., 43, 10,873–10,882, doi:10.1002/2016GL070969

Glessmer, M. S., Eldevik, T., Våge, K. Nilsen, J. E. Ø. & Behrens, E. (2014) Atlantic origin of observed and modelled freshwater anomalies in the Nordic Seas, Nature Geoscience, doi:10.1038/NGEO2259

Graversen, R.G. & Burtu, M. (2016), Arctic amplification enhanced by latent energy transport of atmospheric planetary waves. Q.J.R. Meteorol. Soc., 142: 2046-2054. doi:10.1002/qj.2802

Griffies, Stephen M., et al. (2016) OMIP contribution to CMIP6: experimental and diagnostic protocol for the physical component of the Ocean Model Intercomparison Project. Geoscientific Model Development, 3231-3296, doi:10.5194/gmd-9-3231-2016

Hansen et al. (2016) A stable Faroe Bank Channel overflow 1995-2015. Ocean Science, 12, 1205-1220. doi:10.5194/os-12-1205-2016

Hattermann, T., Isachsen, P. E., von Appen, W.-J., Albretsen, J., & Sundfjord, A. (2016) Eddy driven recirculation of Atlantic Water in Fram Strait, Geophysical Research Letters, 43, 3406–3414, doi:10.1002/2016GL068323.

He, Y. C., Drange, H., Gao, Y., & Bentsen, M. (2016). Simulated Atlantic Meridional Overturning Circulation in the 20th century with an ocean model forced by reanalysis-based atmospheric data sets. Ocean Modelling, 100, 31-48 doi:10.1016/j.ocemod.2015.12.011

Helland-Hansen, B., & Nansen, F. (1909). The Norwegian Sea: Its physical oceanography based upon the Norwegian researches 1900-1904. Kristiania: Det Mallingske bogtrykkeri.

Hopkins, T. S. (1991) The GIN Sea - A synthesis of its physical oceanography and literature review 1972-1985. Earth-Sci. Rev., 3, 1, 175-318. doi:10.1016/0012-8252(91)90001-V

Huang, J., Pickart, R.S., Huang, R.X., Lin, P., Brakstad, A. & Xu, F. (2020) Sources and upstream pathways of the densest overflow water in the Nordic Seas. Nature Communications 11, 5389. doi:10.1038/s41467-020-19050-y

Hunke, E. C., Lipscomb, W. H., Turner, A. K., Jeffery, N., & Elliott, S. (2008). CICE: The Los Alamos sea ice model, documentation and software, version 4.0. Los Alamos National Laboratory Tech. Rep. Los Alamos, NM.

Hurrell, J. W. (1995) Decadal Trends in the North Atlantic Oscillation: Regional Temperatures and Precipitation, Science, 269, doi:10.1126/science.269.5224.676

ICES 2020, International Council for Exploration of the Seas, ICES report on Ocean climate, web: https://ocean.ices.dk/core/iroc

Ilıcak, M. et al. (2016) An assessment of the Arctic Ocean in a suite of interannual CORE-II simulations. Part III: Hydrography and fluxes. Ocean Modelling 100, 141-161, doi:10.1016/j.ocemod.2016.02.004

IHO (1953) International Hydrographic Organization, Limits of Oceans and Seas, Special Publication 28, 3'd edition.

Jakhelln, A. (1936) The Water Transport of Gradient Currents. Geofys. Publ., Vol. XI, p. 11.

Jakobsson, M. & Macnab, R. (2006) A comparison between GEBCO Sheet 5.17 and the International Bathymetric Chart of the Arctic Ocean, Marine Geophysical Researches, 27: 35–48, doi 10.1007/s11001-005-7760-0

Jeansson, E., Olsen, A., Eldevik, T., Skjelvan, I., Omar, A., et al. (2011), The Nordic Seas carbon budget: Sources, sinks and uncertainties. Glob. Biogeochem. Cyc., 25, 4, doi:10.1029/2010GB003961

Jenkins, A. (2011): Convection-Driven Melting near the Grounding Lines of Ice Shelves and Tidewater Glaciers, J. Phys. Oceanogr., 41, 2279–2294, doi:10.1175/JPO-D-11-03.1.

Jochumsen et al. (2017) Revised transport estimates of the Denmark Strait overflow. Journal of Geophysical Research: Oceans, 122, 4, doi:10.1002/2017JC012803.

Johnson, H. L., Cornish, S. B., Kostov, Y., Beer, E. & Lique, C. (2018). Arctic Ocean freshwater content and its decadal memory of sea-level pressure. Geophysical Research Letters, 45, 4991–5001. doi:10.1029/2017GL076870

Jónsson & Valdimarsson (2004) A new path for the Denmark Strait overflow water from the Iceland Sea to Denmark Strait. Geophysical Research Letters, 31, L03305. doi:10.1029/2003GL019214

Karstensen et al., (2005). Water mass transformation in the Greenland Sea during the 1990s. Journal of Geophysical Research, 110, C7. doi:10.1029/2004JC002510

King, M.D., Howat, I.M., Candela, S.G. et al. (2020) Dynamic ice loss from the Greenland Ice Sheet driven by sustained glacier retreat. Commun Earth Environ 1, 1. doi:10.1038/s43247-020-0001-2

Kipp, L. E., M. A. Charette, W. S. Moore, P. B. Henderson, & I. G. Rigor (2018), Increased fluxes of shelf-derived materials to the central Arctic Ocean, Science Advances, 4(1), eaao 1302, doi:10.1126/sciadv.aao1302.

Kolstad, E. W., T. J.Bracegirdle, & I. A.Seierstad (2009) Marine cold-air outbreaks in the North Atlantic: Temporal distribution and associations with large-scale atmospheric circulation. Climate Dyn., 33, 187–197, doi:10.1007/s00382-008-0431-5.

Lannuzel, D., Tedesco, L., Van Leeuwe, M., Campbell, K., Flores, H., Delille, B., & Brown, K. (2020). The future of Arctic sea-ice biogeochemistry and ice-associated ecosystems. *Nature Climate Change*, 1-10. doi:10.1038/s41558-020-00940-4

Latarius, K. & Quadfasel, D. (2016) Water mass transformation in the deep basins of the Nordic Seas: Analyses of heat and freshwater budgets, Deep Sea Research Part 1, 114, 23-42, doi:10.1016/j.dsr.2016.04.012

Lauvset, S.K., Brakstad, A., Våge, K., Olsen, A., Jeansson, E., Mork, K.A. (2018) Continued warming, salinification and oxygenation of the Greenland Sea gyre. Tellus A 70, 1-9. doi:10.1080/16000870.2018.1476434.

Lozier et al. (2019) A sea change in our view of overturning in the subpolar North Atlantic Science 363, 516–521, doi:10.1126/science.aau6592

Li, C. & Born, A. (2019) Coupled atmosphere-ice-ocean dynamics in Dansgaard-Oeschger events, Quaternary Science Reviews 203, doi:10.1016/j.quascirev.2018.10.031

Lique, C. & Thomas, M. D. (2018) Latitudinal shift of the Atlantic Meridional Overturning Circulation source regions under a warming climate. Nature Clim Change 8, 1013–1020. doi:10.1038/s41558-018-0316-5

van der Linden, E. C., Le Bars, D., Bintanja, R. & Hazeleger, W. (2019) Oceanic heat transport into the Arctic under high and low CO2 forcing, Climate Dynamics (2019) 53:4763–4780, doi:10.1007/s00382-019-04824-y

Lindeman, M. R., Straneo, F.,Wilson, N. J., Toole, J. M.,Krishfield, R. A., Beaird, N. L., et al.(2020). Ocean circulation and variability beneath Nioghalvfjerdsbræ (79 North Glacier) ice tongue. Journal of Geophysical Research: Oceans, 125, e2020JC016091. doi:10.1029/2020JC016091

Marshall, J. & Schott, F. (1999) Open - ocean convection: Observations, theory, and models. Reviews of Geophysics 37, 1-64. doi:10.1029/98RG02739.

Mastropole, D., Pickart, R.S., Valdimarsson, H., Våge, K., Jochumsen, K., Girton, J. (2017) On the hydrography of Denmark Strait. Journal of Geophysical Research 122, 306-321. doi:10.1002/2016JC012007.

Mauritzen, C. (1996) Production of dense overflow waters feeding the North Atlantic across the Greenland-Scotland Ridge. Part 1: Evidence for a revised circulation scheme. Deep Sea Res. Part I Oceanogr. Res. Pap. 43, 769-806, doi:10.1016/0967-0637(96)00037-4.

Mayer, M., S. Tietsche, L. Haimberger, T. Tsubouchi, J. Mayer, & H. Zuo (2019): An Improved Estimate of the Coupled Arctic Energy Budget. J. Climate, 32, 7915–7934, doi:10.1175/JCLI-D-19-0233.1

Meier, W. N., et al. (2014), Arctic sea ice in transformation: A review of recent observed changes and impacts on biology and human activity, Rev. Geophys., 52, 185– 217, doi:10.1002/2013RG000431.

Michel, C., Rivière, G., Terray, L., & Joly, B. (2012). The dynamical link between surface cyclones, upper-tropospheric Rossby wave breaking and the life cycle of the Scandinavian blocking. Geophysical research letters, 39 (10) doi:10.1029/2012GL051682

Moore, G.W.K., Våge, K., Pickart, R. S., & Renfrew, I. A. (2015). Decreasing intensity of open-ocean convection in the Greenland and Iceland seas, Nature Climate Change, 5, 877-882. doi:10.1038/nclimate2688.

Mork, K. A., Ø. Skagseth, V. Ivshin, V.Ozhigin,S. L. Hughes, & H. Valdimarsson (2014), Advective and atmospheric forced changes in heat and fresh water content in the Norwegian Sea, 1951–2010, Geophys. Res. Lett., 41, 6221–6228, doi:10.1002/2014GL061038.

Mork, K. A., Skagseth, Ø. & Søiland, H. (2019) Recent warming and freshening of the Norwegian Sea observed by Argo data. J. Clim. 32, 3695–3705, doi:10.1175/JCLI-D-18-0591.1.

Mouginot, J., Rignot, E., Scheuchl, B., Fenty, I., Khazendar, A., Morlighem, M.,…Paden, J. (2015). Fast retreat of Zachariæ Isstrøm, northeast Greenland. Science, 350(6266), 1357–1361. doi:10.1126/science.aac7111

Mouginot, J., Rignot, E., Bjørk, A. A., van den Broeke, M., Millan, R., Morlighem, M., Noël, B., Scheuchl, B. & Wood, M. (2019) Forty-six years of Greenland Ice Sheet mass balance from 1972 to 2018, Proceedings of the National Academy of Sciences May 2019, 116 (19) 9239-9244; doi: 10.1073/pnas.1904242116

Mosby, H. (1962). Water, Salt and Heat Balance of the North Polar Sea and the Norwegian Sea. Vitenskapsakademiet.

Muilwijk, M., Smedsrud, L. H., Ilicak, M.,& Drange, H. (2018). Atlantic Water heat transport variability in the 20th century Arctic Ocean from a global ocean model and observations. JGR Oceans, 123, 8159–8179, doi:10.1029/2018JC014327

Muilwijk, M., Ilicak, M., Cornish, S. B., Danilov, S., Gelderloos, R., Gerdes, R., et al. (2019). Arctic Ocean response to Greenland Sea wind anomalies in a suite of model simulations. Journal of Geophysical Research: Oceans, 124, doi:10.1029/2019JC015101

NCSC 2020, Norwegian Climate Service Centre, Observations and weather statistics, web: https://klimaservicesenter.no/observations/

Nilsen, J. E. Ø., Y. Gao, H. Drange, T. Furevik, & M. Bentsen (2003) Simulated North Atlantic-Nordic Seas water mass exchanges in an isopycnic coordinate OGCM, Geophys. Res. Lett., 30(10), 1536, doi:10.1029/2002GL016597.

Nguyen, A. T., Pillar, H., Ocaña, V., Bigdeli, A., Smith, T. A. & Heimbach, P. (2020) The Arctic Subpolar gyre sTate Estimate (ASTE): Description and assessment of a data-constrained, dynamically consistent ocean-sea ice estimate for 2002-2017, submitted to Journal of Advances in Modeling Earth Systems (JAMES), doi:10.1002/essoar.10504669.3

Nilsen, J. E. Ø., Hátún, H., Mork, K. A., Valdimarsson, H. (2008). The NISE Dataset. Technical Report 08-01. Faroese Fisheries Laboratory, Box 3051, Tórshavn Faroe Islands.

NMDC 2020, Norwegian Marine Data Centre, Data sets, web: https://nmdc.no/nmdc/datasets

Notz, D. & Stroeve, J. (2016). Observed Arctic sea-ice loss directly follows anthropogenic CO2 emission. Science, 354, 747–750, doi:10.1126/science.aag2345

Nøst, O. A., & Isachsen, P. E. (2003). The large-scale time-mean ocean circulation in the Nordic Seas and Arctic Ocean estimated from simplified dynamics. Journal of Marine Research, 61(2), 175–210. doi:10.1357/002224003322005069

Onarheim, I.H., Eldevik, T., Smedsrud, L. H. & Stroeve, J. C. (2018). Seasonal and regional manifestation of Arctic sea ice loss. Journal of Climate, 31, 4917–4932, doi:10.1175/JCLI-D-17-0427.1

Orvik, K.A., Skagseth, Ø. & Mork, M. (2001) Atlantic inflow to the Nordic Seas: current structure and volume fluxes from moored current meters, VM-ADCP and SeaSoar-CTD observations, 1995–1999, Deep Sea Research Part I: Oceanographic Research Papers, 48, 4, 937-957, doi:10.1016/S0967-0637(00)00038-8

Oudar, T., Cattiaux, J., & Douville, H. (2020). Drivers of the northern extratropical eddy-driven jet change in CMIP5 and CMIP6 models. Geophysical Research Letters, 47, e2019GL086695. doi:10.1029/2019GL086695

Overland, J. E., Turet, P., & Oort, A. H. (1996). Regional variations of moist static energy flux into the Arctic. Journal of Climate, 9, 54–65, doi:10.1175/1520-0442(1996)009<0054:RVOMSE>2.0.CO;2

Papritz, L., & Grams, C. M. (2018). Linking low-frequency large-scale circulation patterns to cold air outbreak formation in the northeastern North Atlantic. Geophysical Research Letters, 45(5), 2542-2553, doi:10.1002/2017GL076921

Papritz, L., & Spengler, T. (2017). A Lagrangian climatology of wintertime cold air outbreaks in the Irminger and Nordic seas and their role in shaping air-sea heat fluxes. Journal of Climate, 30, 2717–2737. doi:10.1175/JCLI-D-16-0605.1

Papritz, L. (2017). Synoptic environments and characteristics of cold air outbreaks in the Irminger Sea. International Journal of Climatology, 37, 193-207, doi:10.1002/joc.4991

Pérez-Hernández et al. (2019) Structure, Transport, and Seasonality of the Atlantic Water Boundary Current North of Svalbard: Results From a Yearlong Mooring Array. Journal of Geophysical Research: Oceans, 124, 3. doi:10.1029/2018JC014759

Perovich, D. K., Light, B., Eicken, H., Jones, K. F., Runciman, K., Nghiem, S. V. (2007). Increasing solar heating of the Arctic Ocean and adjacent seas, 1979–2005: Attribution and role in the ice-albedo feedback. Geophysical Research Letters, 34, L19505, doi:10.1029/2007GL031480.

Peixoto, J., & Oort, A. H. (1992). Physics of Climate: American Institute of Physics.

Pithan, F., Mauritsen, T. (2014). Arctic amplification dominated by temperature feedbacks in contemporary climate models. Nature Geoscience, 7, 181–184, doi:10.1038/ngeo2071

Pistone, K., Eisenman, I., & Ramanathan, V. (2019). Radiative heating of an ice-free Arctic Ocean. Geophysical Research Letters, 46, 7474–7480 doi:10.1029/2019GL082914

Polyakov et al.(2017) Greater role for Atlantic inflows on sea-ice loss in the Eurasian Basin of the Arctic Ocean, Science doi:10.1126/science.aai8204.

Rayner, N. A., Parker, D. E., Horton, E. B., Folland, C. K., Alexander, L. V., Rowell, D. P., Kent, E. C., and Kaplan, A. (2003), Global analyses of sea surface temperature, sea ice, and night marine air temperature since the late nineteenth century, *J. Geophys. Res.*, 108, 4407, doi:10.1029/2002JD002670, D14.

Rossby, T., Flagg, C., Chafik, L., Harden, B., & Søiland, H. (2018). A direct estimate of volume, heat, and freshwater exchange across the Greenland-Iceland-Faroe-Scotland Ridge. Journal of Geophysical Research: Oceans, 123, 7139–7153, doi:10.1029/2018JC014250

Rossby, T., Chafik, L., & Houpert, L. (2020). What can hydrography tell us about the strength of the Nordic Seas MOC over the last 70 to 100 years?. Geophysical Research Letters, 47, e2020GL087456. doi:10.1029/2020GL087456

Ruggieri, P., Alvarez-Castro, M. C., Athanasiadis, P., Bellucci, A., Materia, S., & Gualdi, S. (2020). North Atlantic circulation regimes and heat transport by synoptic eddies. Journal of Climate, 33(11), 4769-4785, doi:10.1175/JCLI-D-19-0498.1

Rysgaard, S., Sogaard, D. H., Cooper, M., Pucko, M., Lennert, K., Papakyriakou, T. N., Wang, F., Geilfus, N. X., Glud, R. N., Ehn, J., McGinnis, D. F., Attard, K., Sievers, J., Deming, J. W., & Barber, D. (2013) Ikaite crystal distribution in winter sea ice and implications for CO2 system dynamics, The Cryosphere, 7, 707-718, doi:10.5194/tc-7-707-2013

Schaffer, J., Kanzow, T. von Appen, W. et al. (2020) Bathymetry constrains ocean heat supply to Greenland's largest glacier tongue. Nat. Geosci. doi:10.1038/s41561-019-0529-x

Schweiger, A.J., K.R. Wood, & J. Zhang (2019) Arctic Sea Ice Volume Variability over 1901–2010: A Model-Based Reconstruction. J. Climate, 32, 4731–4752, doi:10.1175/JCLI-D-19-0008.1

Segtnan, O. H., T. Furevik, & A. D. Jenkins (2011), Heat and freshwater budgets of the Nordic seas computed from atmospheric reanalysis and ocean observations, J. Geophys. Res., 116, C11003, doi:10.1029/2011JC006939.

Seierstad, I. A., Stephenson, D. B., & Kvamstø, N. G. (2007). How useful are teleconnection patterns for explaining variability in extratropical storminess? Tellus A: Dynamic Meteorology and Oceanography, *59* (2), 170-181, doi:10.1111/j.1600-0870.2007.00226.x

Selyuzhenok, V., Bashmachnikov, I., Ricker, R., Vesman, A., & Bobylev, L. (2020) Sea ice volume variability and water temperature in the Greenland Sea. The Cryosphere, 14, 477-495. doi:10.5194/tc-14-477-2020

Semper, S., Våge, K., Pickart, R.S., Valdimarsson, H., Torres, D.J. & Jónsson, S. (2019) The emergence of the North Icelandic Jet and its evolution from northeast Iceland to Denmark Strait. Journal of Physical Oceanography. doi:10.1175/JPO-D-19-0088.1.

Semper, S., Pickart, R.S., Våge, K., Larsen, K.M.H., Hátún, H. & Hansen, B. (2020) The Iceland-Faroe Slope Jet: a conduit for dense water toward the Faroe Bank Channel overflow. Nature Communications 11, 5390. doi:10.1038/s41467-020-19049-5

Skagseth, Ø. T. Eldevik, M. Årthun, H. Asbjørnsen, V. Lien & L. H. Smedsrud (2020) Reduced efficiency of the Barents Sea cooling machine. Nature Climate Change, 2020, doi:10.1038/s41558-020-0772-6

Slater, D. A., Straneo, F., Felikson, D., Little, C. M., Goelzer, H., Fettweis, X., and Holte, J. (2019) Estimating Greenland tidewater glacier retreat driven by submarine melting, The Cryosphere, 13, 2489–2509, doi:10.5194/tc-13-2489-2019.

Slater, D. A., Goldberg, D. N., Nienow, P. W., & Cowton, T. R. (2016): Scalings for submarine melting at tidewater glaciers from buoyant plume theory, J. Phys. Oceanogr., 46, 1839–1855, doi:0.1175/JPO-D-15-0132.1.

Simonsen, K., & P. M. Haugan (1996), Heat budgets for the Arctic Mediterranean and sea surface heat flux parameterizations for the Nordic Seas, J. Geophys. Res., 101, 6553–6576, doi:10.1029/95JC03305

Smedsrud, L. H., et al. (2013), The role of the Barents Sea in the Arctic climate system, Rev. Geophys., 51, doi:10.1002/rog.20017.

Straneo, F., Sutherland, D.A., Holland, D., Gladish, C., Hamilton, G.S., Johnson, H.L., Rignot, E., Xu, Y. & Koppes, M. (2012) Characteristics of ocean waters reaching Greenland's glaciers. *Annals of Glaciology*, *53*(60), 202-210, doi:10.3189/2012AoG60A059

Straneo, F. & Heimbach, P. (2013) North Atlantic warming and the retreat of Greenland's outlet glaciers. Nature 504, 36–43 doi:10.1038/nature12854

Stocker, A.N., Renner, A.H. & Knol-Kauffman, M., 2020. Sea ice variability and maritime activity around Svalbard in the period 2012–2019. *Scientific reports*, *10*(1), pp.1-12, doi:10.1038/s41598-020-74064-2

Spall, M.A. (2004): Boundary Currents and Watermass Transformation in Marginal Seas. J. Phys. Oceanogr., 34, 1197–1213, doi:10.1175/1520-0485

Sverdrup, H.U., Johnson, M.W., Fleming, R.H. (1942) The Oceans: Their Physics, Chemistry and General Biology. Prentice-Hall, New York, 1042 pp.

Swift, J.H. & Aagaard, K. (1981) Seasonal transitions and water mass formation in the Iceland and Greenland seas. Deep-Sea Research A 28, 1107-1129. doi:10.1016/0198-0149(81)90050-9.

Takahashi, T., Olafsson, J., Goddard, J. G., Chipman, D. W., & Sutherland, S. C. (1993) Seasonal-Variation of Co2 and Nutrients in the High-Latitude Surface Oceans - a Comparative-Study, Global Biogeochem Cy, 7, 843-878, doi:10.1029/93GB02263

Timmermans, M.-L., & Marshall, J. (2020) Understanding Arctic Ocean circulation: A review of ocean dynamics in a changing climate. Journal of Geophysical Research: Oceans, 125, e2018JC014378. doi:10.1029/2018JC014378

Tsujino, Hiroyuki, et al. (2018) JRA-55 based surface dataset for driving ocean–sea-ice models (JRA55-do), Ocean Modelling 130, 79-139, doi:10.1016/j.ocemod.2018.07.002

Trenberth, K. E., & Shea, D. J. (2006). Atlantic hurricanes and natural variability in 2005. Geophysical Research Letters, 33, L12704. doi:10.1029/2006GL026894

Trenberth, K. E., & Fasullo, J. T. (2017). Atlantic meridional heat transports computed from balancing Earth's energy locally. Geoph. Res. Lett., 44(4), 1919-1927, doi:10.1002/2016GL072475

Trenberth, K. E., Zhang, Y., Fasullo, J. T., & Cheng, L. (2019). Observation-based estimates of global and basin ocean meridional heat transport time series. J. Climate, 32, 4567-4583, doi:10.1175/JCLI-D-18-0872.1

Trigo, R.M., Valente, M.A., Trigo, I.F., Miranda, P.M.A., Ramos, A.M., Paredes, D. & García-Herrera, R. (2008). The Impact of North Atlantic Wind and Cyclone Trends on European Precipitation and Significant Wave Height in the Atlantic. Annals of the New York Academy of Sciences, 1146: 212-234. doi:10.1196/annals.1446.014

Tsubouchi, T. et. al (2020) Increased ocean heat transport into the Nordic Seas and Arctic Ocean over the period 1993-2016. Nature Climate Change, doi:10.1038/s41558-020-00941-3

Vikebø, F. et al. (2003) Wave height variations in the North Sea and on the Norwegian Continental Shelf, 1881–1999, Continental Shelf Research 23 (2003) 251–263. doi:10.1016/S0278-4343(02)00210-8

Visbeck et al., 1995. Preconditioning the Greenland Sea for deep convection: ice formation and ice drift. Journal of Geophysical Research: Oceans, 100, C9, doi: 10.1029/95JC01611.

Våge, K., Pickart, R.S., Spall, M.A., Valdimarsson, H., Jónsson, S., Torres, D.J., Østerhus, S., Eldevik, T. (2011) Significant role of the North Icelandic Jet in the formation of Denmark Strait overflow water. Nature Geoscience 4, 723-727. doi:10.1038/ngeo1234.

Våge, K. et al. (2015) Water mass transformation in the Iceland Sea, Deep Sea Research, 101, 98-109, doi:10.1016/j.dsr.2015.04.001.

Våge K., L. Papritz, L. Håvik, M.A. Spall, & G.W.K. Moore (2018) Ocean convection linked to the recent ice edge retreat along east Greenland. Nature Communications, 9, doi:10.1038/s41467-018-03468-6

Walsh, J. E. F. Fetterer, J. S. Stewart, & W. L. Chapman (2017) A database for depicting Arctic sea ice variations back to 1850. Geogr. Rev., 107, 89–107, doi:10.1111/j.1931-0846.2016.12195.x.

Watson, A.J., P.D. Nightingale, & D. J. Cooper (1995) Modelling atmosphere-ocean CO2 transfer, Phil. Trans. R. Soc. Lond. B, 348, 125-132, doi:10.1098/rstb.1995.0054

Wernli, H. & C. Schwierz (2006) Surface Cyclones in the ERA-40 Dataset (1958–2001). Part I: Novel Identification Method and Global Climatology. J. Atmos. Sci., 63, 2486–2507, doi:10.1175/JAS3766.1

Werenskiold, W. (1935) Coastal Currents. Geofys. Publ., Vol. X, p. 13.

Wettstein, J. J., & Wallace, J. M. (2010). Observed patterns of month-to-month storm-track variability and their relationship to the background flow. Journal of the Atmospheric Sciences, 67(5), 1420-1437, doi:10.1175/2009JAS3194.1

Woodgate, R. A., Aagaard, K., Weingartner, T. J. (2006). Interannual changes in the Bering Strait fluxes of volume, heat and freshwater between 1991 and 2004. Geophysical Research Letters, 33, L15609. doi:10.1029/2006GL026931

Woollings, T., Hannachi, A., & Hoskins, B. (2010). Variability of the North Atlantic eddy-driven jet stream. Quarterly Journal of the Royal Meteorological Society, 136(649), 856-868, doi:10.1002/qj.625

Wunsch, C., 2020: Is the Ocean Speeding Up? Ocean Surface Energy Trends. J. Phys. Oceanogr., 50, 3205–3217, doi:10.1175/JPO-D-20-0082.1.

Yashayaev, I. & Seidov, D. (2015) The role of the Atlantic Water in multidecadal ocean variability in the Nordic and Barents Seas. Prog. Oceanogr. 132, 68–127, doi:10.1016/j.pocean.2014.11.009

Yasunaka, S., Siswanto, E., Olsen, A., Hoppema, M., Watanabe, E., Fransson, A., Chierici, M., Murata, A., Lauvset, S. K., Wanninkhof, R., Takahashi, T., Kosugi, N., Omar, A. M., van Heuven, S., and Mathis, J. T. (2018) Arctic Ocean CO2 uptake: an improved multiyear estimate of the air–sea CO2 flux incorporating chlorophyll a concentrations, Biogeosciences, 15, 1643–1661, doi:10.5194/bg-15-1643-2018.

Young, I. R. & Ribal, A. (2019) Multiplatform evaluation of global trends in wind speed and wave height, Science, Vol. 364, Issue 6440, pp. 548-552, doi: 10.1126/science.aav9527

Østerhus, S. et al. (2019) Arctic Mediterranean exchanges: a consistent volume budget and trends in transports from two decades of observations, Ocean Sci., 15, 379-399, doi:10.5194/os-15-379-2019

Årthun, M., T. Eldevik, L. H. Smedsrud, Ø. Skagseth, & R. Ingvaldsen (2012), Quantifying the influence of Atlantic heat on Barents Sea ice variability and retreat, J. Clim., 25, 4736–4743, doi:10.1175/JCLI-D-11-00466.1.

Årthun, M. & Eldevik, T. (2016) On Anomalous Ocean Heat Transport toward the Arctic and Associated Climate Predictability, J.lim. 29(2), 689–704, doi:10.1175/JCLI-D-15-0448.1

Wilson, N. J. & F. Straneo (2015), Water exchange between the continental shelf and the cavity beneath Nioghalvfjerdsbræ (79 North Glacier), Geophys. Res. Lett., 42, 7648–7654, doi:10.1002/2015GL064944